ACKNOWLEDGMENTS

The author wishes to express his gratitude and deep appreciation to his thesis supervisor, Dr. T.S. Sankar, for initiating the project and providing continued guidance throughout the investigation. The author extends his gratitude to his employers, Transport Canada, Aeronautical Engineering Division, for their comprehension and support during his work. He also wants to express his sincere thanks to Miss Clo Leone for her careful typing of the manuscript.

TABLE OF CONTENTS

LIST OF FIGURES

NOMENCLATURE

a	undeformed radius
B & C	parameters defined by (3.24)
D	flextural rigidity $= Eh^3/12(1-\nu^2)$
D_f	dissipative function
ds	element of undeformed meridian
ds_d	element of deformed meridian
e	strain due to axial shortening
E	Young's modulus
f	$(\pi/\alpha)\beta$
g	$(\pi/\alpha)^3 u$
h	shell thickness
H	height of potential barrier
K_1	parameter $= (2\sqrt{1-\nu^2}\,h)/(\sqrt{3}\,p_{cr}\,a^4\alpha)$
K'	parameter $= (3\pi^4 D_f \ell)/(2a^3\alpha^3 h^2)$
$\bar{K}$	parameter $= (\frac{m\,h^2}{2})(K'h^4)$
ℓ	length of panel
L	normalized displaced volume
L_a	volume displaced during deformation
L_o	snap-through displaced volume
L, M & N	parameters defined by (3.35)
m	mass of panel
M_x	meridional moment resultant
M_θ	circumferential moment resultant
N_x	meridional stress resultant
N_θ	circumferential stress resultant
P_T	first probability of buckling at time T
p	external pressure

q_i	displacement of shell
Q	transverse shear
Q_i	generalized force
r	horizontal distance from axis of symmetry to point on middle surface
R_1	radius of curvature of deformed meridian
R_2	radius of curvature of deformed surface in direction tangent to circumference
R_T	reliability figure
S & T	defined by (2.43) Ch. II
T	kinetic energy Ch. III
T	time interval for first probability of buckling Ch. III & IV
u & w	dimensionless displacement
U & W	dimensionless displacement
u_a & U_a	tangential displacement Fig. (2.3)
V	total potential energy
V_b	bending strain energy
V_m	membrane strain energy
V_p	work done by external pressure
w_a & W_a	normal displacements Fig. (2.3)
x	meridional coordinate
,x	differentiation with respect to x
y	$(\pi/\alpha)x$
,y	differentiation with respect to y
z	vertical distance from apex to point on middle surface
α	sustained angle

β	negative angle of rotation of meridional tangent during deformation
β_o	viscous damping coefficient
$\overline{\beta}$	β_o/m
γ	nondimensional damping coefficient
ε_x & ε_θ	meridional and circumferential strain
ζ_i	nondimensional displacement = q_i/h
θ	angle of transformation
κ_1 & κ_2	meridional and circumferential change in curvature
λ	geometric parameter given by (2.38) Ch. II
λ	static load parameter = λ'/h Ch. III & IV
λ'	static load parameter
ν	Poisson's ratio
$\xi(t)$	generalized force function
ρ	pressure parameter = p/p_{cr}
$\overline{\rho}$	density of panel
τ_1	period of fundamental frequency
ϕ	angle from edge to element
ω_1	natural frequency of panel

CHAPTER I

INTRODUCTION

Chapter I

INTRODUCTION

Recent interest in design and fabrication of pressure hulls for deep sea exploration, pressure vessels in nuclear application as well as special shell forms in aeronautical application has led a great number of investigations to study the behaviour of shells under deterministic external pressure loading. Only Sankar and Ariaratnam [1, 2, 3] tackled a similar problem from the stochastic point of view. They investigated simple structures such as an arch to calculate the probability of the time of the first snap-through of a structure under randomly varying loads from a given initial state as well as the probability of the first snap-through in a given time.

The purpose of this study is to extend the existing probabilistic analysis to determine the stability of three-dimensional structures like thin cylindrical panels and spherical shells under random loads. Only in the domain of aeronautics designers make extensive use of such theories in their designs. Application could vary from designing unpressurized airframe panels which exist on all airplanes, to specifically designed domes carrying special research equipments. Aircraft protrusions are extensively used in air survey programs such as ice patrol, pollution control around large cities, detection of oil fields, etc. .... These structures are subjected to large variation of randomly

applied external pressures consisting of aerodynamic, clear air turbulance and air gusts pressures. Also, randomly distributed initial imperfections in the shells are known to contribute highly to the lowering of the buckling stresses. Deep sea pressure hulls, altitude test chambers, nuclear pressure vessels, etc. ... are among other fields which could make use of such an analysis in their design.

In order to make this presentation self-contained, a historical survey on the large displacement theory, the energy method used for a buckling solution are given and are followed by the Sankar, Ariaratnam probability analysis of first snap-through and snap-buckling applied to cylindrical panels and spherical shells.

The development of the large displacement theory started prior to the first World War when Lorenz [4], Timoshenko [5] and Southwell [6] developed the classical solution of the linear equations governing the neutral equilibrium of an axially compressed cylindrical shell. The experimental work done on the subject in the early thirties showed that shells buckle under much smaller stresses than those predicted by the classical theory.

In the early forties, von Karman [7] demonstrated that the analysis of the buckling of the shells by means of the small-displacement theory was not sufficient to establish the practical limits of the load carrying capacity of thin shells. Later, with the collaboration of Donnel [16],

von Karman analysed the problem by means of large displacement equations and was able then to find solutions involving large-displacements coexisting with small-displacements under smaller critical loads than those given by the classical theory. In fact, for each pressure load condition, three displacements could be determined; a small displacement corresponding to a stable unbuckle state, a large one corresponding to a stable buckle state, and a third in between the other two mentioned above, but corresponding to an unstable state. The physical reasoning behind the multiple solution of the large displacement equation is the existence of polyhedral surfaces into which the cylindrical shell can be developed, such that every element of the shell is transformed into a corresponding element of the polyhedron. These solutions were described by Yoshimura [8] and Kfrste [9].

A shortcoming of the large displacement approach was in wide disagreement between the calculated critical loads and the experimentally observed ones. Also, the experimentally obtained buckling stresses decreased more rapidly with increasing value of radius-to-wall thickness ratio than predicted by the theory. This rapid decrease in the buckling load was caused by manufacturing defects in the shell geometry.

On the subject of shell imperfections, Flügge [10] carried out calculations as early as 1932, in order to confirm whether deviations of certain magnitudes could account for the differences between experimental and theoretical buckling stresses.

His lack of success came from the restricted scope of his study.

Later in 1945 Koiter [11] succeeded, with a broader analysis on the general theory of the stability of thin shells, to show that the slope of the load versus end shortening curve could be positive, zero or negative. He showed that shells are extremely sensitive to initial imperfections and that they do snap into a large-displacement state of equilibrium associated with a sudden drop in load well before the classical value of the critical stress is reached.

In 1963, Koiter [12] modified the classical buckling formula by introducing a correction factor implicitly defined in relation to Poisson's ratio, the shell thickness, its radius and the ratio of amplitude of initial deviations to the wall thickness. This gave buckling stresses in agreement with the experimental observations provided that the amplitude of the deviations from sphericity are proportional to the radius of the shell.

Again von Karman with Tsien [13] in 1939 made the first attempt at developing a large-displacement theory, for spherical shells, in order to explain the differences between theoretical and experimental critical buckling stresses. Having observed that the size of buckles were relatively small compared to the diameter of the shell, Karman and Tsien made use of the large-displacement equations valid for shallow shells together with corresponding energy expression to study

the behaviour of shallow spherical caps clamped around the edge. It was conjunctured and later shown analytically by means of an example that the load-displacement curve for that type of shell segment consisted of three parts, a stable unbuckled and a stable buckled state where the displacement increases with an increment in the load, and an unstable state where the displacement increases with a decrease in the load, as explained in figure (2.1). From here the problem of buckling related to spherical shells took quite a different character from that of the classical theory.

Suppose the buckling pressure is deemed to have been reached when a small inward dimple occurs at the surface of a perfect spherical shell. The classical theory is correct in stating that up to the "classical buckling load", any infinitesimal deviation from the spherical form involves an increase in the potential energy of the shell. At this point, the structure is said to be stable. However, along the unbuckled state the theory fails to reveal that there are configurations with finite displacements involving a lower potential energy level than the classical maximum. In these configurations the shell may snap-buckle and jump from the unbuckled state of equilibrium to another buckled stable state at the same or even at a lower load level.

A large number of investigators used the above approach in conjunction with Reissner's [14] leading equations on the axisymmetrical deformation of thin shells. Two of the most

complete studies on the buckling of shallow spherical shells were by Budiansky [27], and by Weinitschke [23] who made use of two matched infinite series to satisfy Reissner's equations. They found that most of the available experimental results were far below the theoretical curves and attributed this discrepancy to the random imperfections in the shell shape. The difference in buckling stresses decreased significantly when Krenzke and Kiernan [15] reported tests on specimens prepared with extreme care.

The methods used in the case of buckling of spherical shells can be classified in the following five types:

1. The perturbation method [17, 18] where the non-dimensional radial deflection at the centre of the shell is employed as a perturbation parameter.
2. The power series method [19 to 23], in which the solution of the load displacement equation is achieved by representing the equation as a power series and determining its coefficients using Newton-Raphson iteration process.
3. The finite difference method [24, 25, 26] in which the load-displacement equations for shallow shells are solved by applying the finite difference technique. Bushnell [32, 35] solved the finite difference analog of the differential equations by using variable static spacing in order to obtain accurate predictions of edge stresses and displacements.

4. The iterative numerical integration method [27 to 31] in which the load-displacement non-linear differential equations are solved numerically by approximating them by a sequence of linear variational equations. The linearization is performed by expanding non-linear terms in the differential equation in a Taylor series and retaining only the linear terms.
5. The energy method [32] is used to locate points on the unstable branch of the load-displacement curve, and to determine the effect of imperfections in the initial shape of the spherical shell. It involves an evaluation of the potential expression in terms of the tangential and normal displacements which are expressed as simple trigonometric series. Once the non-linear algebraic equations resulting from the minimization of the potential energy with respect to each of the undetermined coefficients are solved, load-deflection curves can be plotted for various values of a geometric parameter of the shell for perfect shells as well as for shells with initial deviation from sphericity.

The problems of interest in the stochastic case are the determination of the probability of the time of the first snap-through of a structure starting from a given initial state and of the probability of the first snap-through in a given time. A shell type structure whose initial rise is small and loses its stability under a single symmetric mode of deformation, constitutes a good example of snap-through.

In the late thirties Kramers [33], in his study of kinetics of chemical reaction, calculated the probability of escape of particles over a potential barrier through the shuttling action of Brownian forces caused by a surrounding medium in temperature equilibrium. In order to study the probability of snap-through of cylindrical panels under random pressure Goncharenko [34] adapted a simplified Kramers method. Later Ariaratnam and Sankar [1] extended it to derive the probability of the first symmetric snap-through in a finite time using the locally stationary solution of the Fokker-Planck equation for stochastically loaded shallow arches.

In the snap-through process, the potential energy function has a single local maximum corresponding to an unstable equilibrium configuration. For structures subjected to stochastic load, the problem involves the determination of the diffusion rate of the probability density across the potential hump (maximum of the potential energy curve). Later, Ariaratnam and Sankar [2] extended their study to shell-type structures whose initial rise exceeded a certain specific value; these types present a symmetric and an antisymmetric mode of deformation and display a snap-buckling type of instability at a critical loading. In this case the potential energy surface has a saddle point and represents the unstable equilibrium state of the structure. Under stochastic load, the problem involves a discussion of the diffusion of the probability density in a four-dimensional phase space. Finally, Ariaratnam and Sankar [3] extended the above analysis to the practical

problem of asymmetric dynamic instability of shallow arches.

The purpose of this study is to extend Sankar and Ariaratnam's [1, 2, 3] work on the probability of first snap buckling of cylindrical panels and spherical caps under stochastic loads. In the case of cylindrical panels under random surface loading Sankar's [40] approach will be used as the basis for the discussion. The equations of motion will be written in terms of the potential energy using Lagrange's equations of motion. Then the energy surface will be defined and the diffusion of the probability density discussed, leading to the determination of the first probability of buckling in a given time. The structural analysis of the spherical caps will be developed using the energy method and an extension to the first probability of buckling for panels will be proposed.

CHAPTER II

DYNAMICS OF SHALLOW SPHERICAL CAPS

Chapter II

DYNAMICS OF SHALLOW SPHERICAL CAPS

2.1 Introduction

The purpose of this chapter is to derive possible expressions for the potential energy of spherical caps. These expressions can be used to extend the earlier work done by Sankar and Ariaratnam [1, 2, 3] on the stochastic analysis of the instability of spherical caps.

Reissner's [14] basic equilibrium approach and Bushnell's [32] potential energy approach, to the dynamics of shallow spherical caps, was based on the strain-displacement and curvature-displacement relations. The energy expression developed by Bushnell [32] is a logical extension of the equilibrium approach [14] to the dynamics of spherical caps, and should be developed first in order to give a comprehensive view of the matter.

Bushnell [32] actually solved the simplified Reissner equations, plotting the stable branches of the load-deflection curve and then used the potential energy to complete the unstable part, as shown in figure (2.1).

The effect of imperfections, which drastically reduces the classically arrived buckling loads was also dealt with by Bushnell [32] as an extended application of his potential energy approach. These effects are shown in figures (2.1) and (2.2).

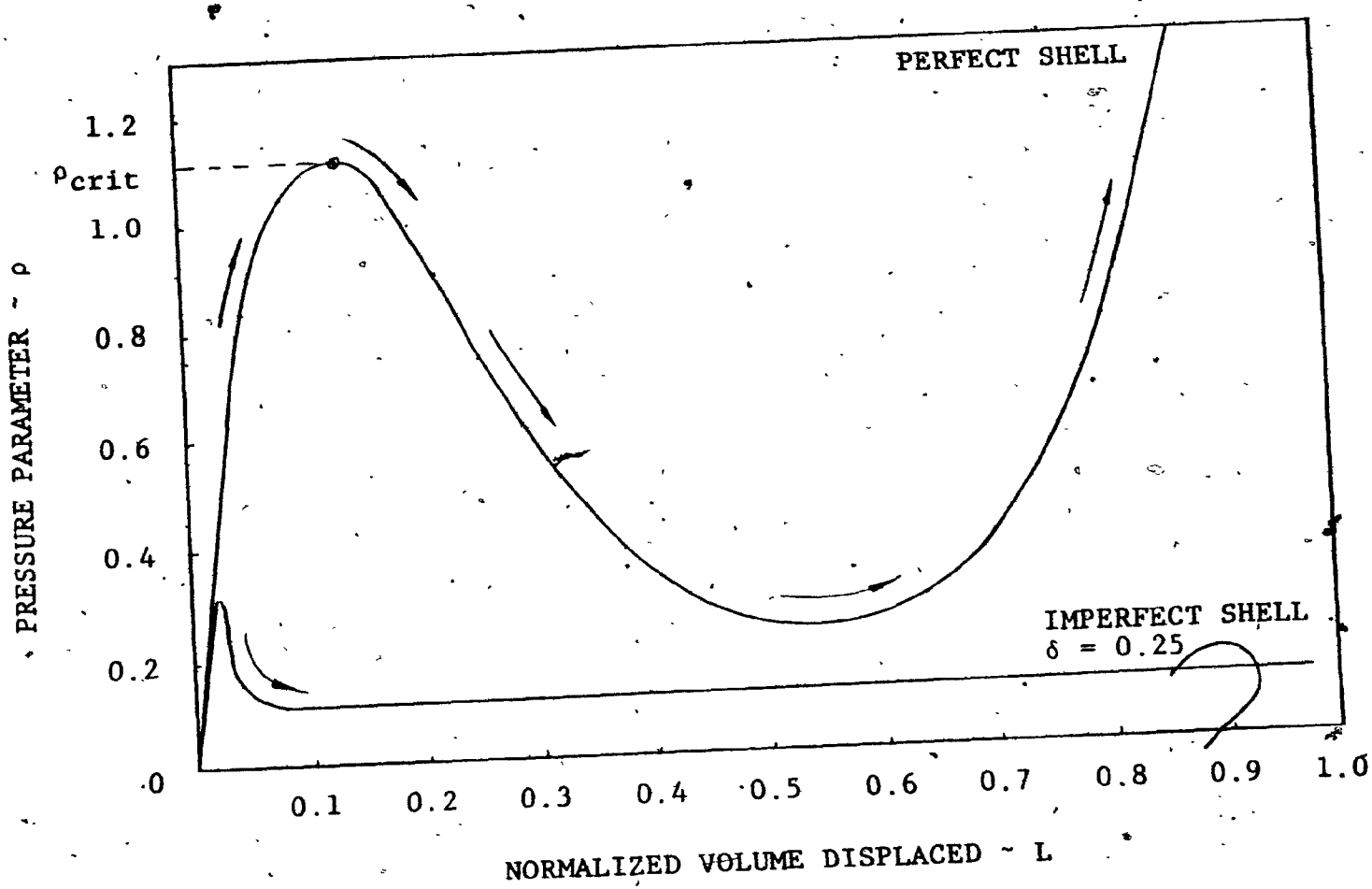

FIG. 2.1 Load-Deflection Curves for Perfect and Imperfect Shells

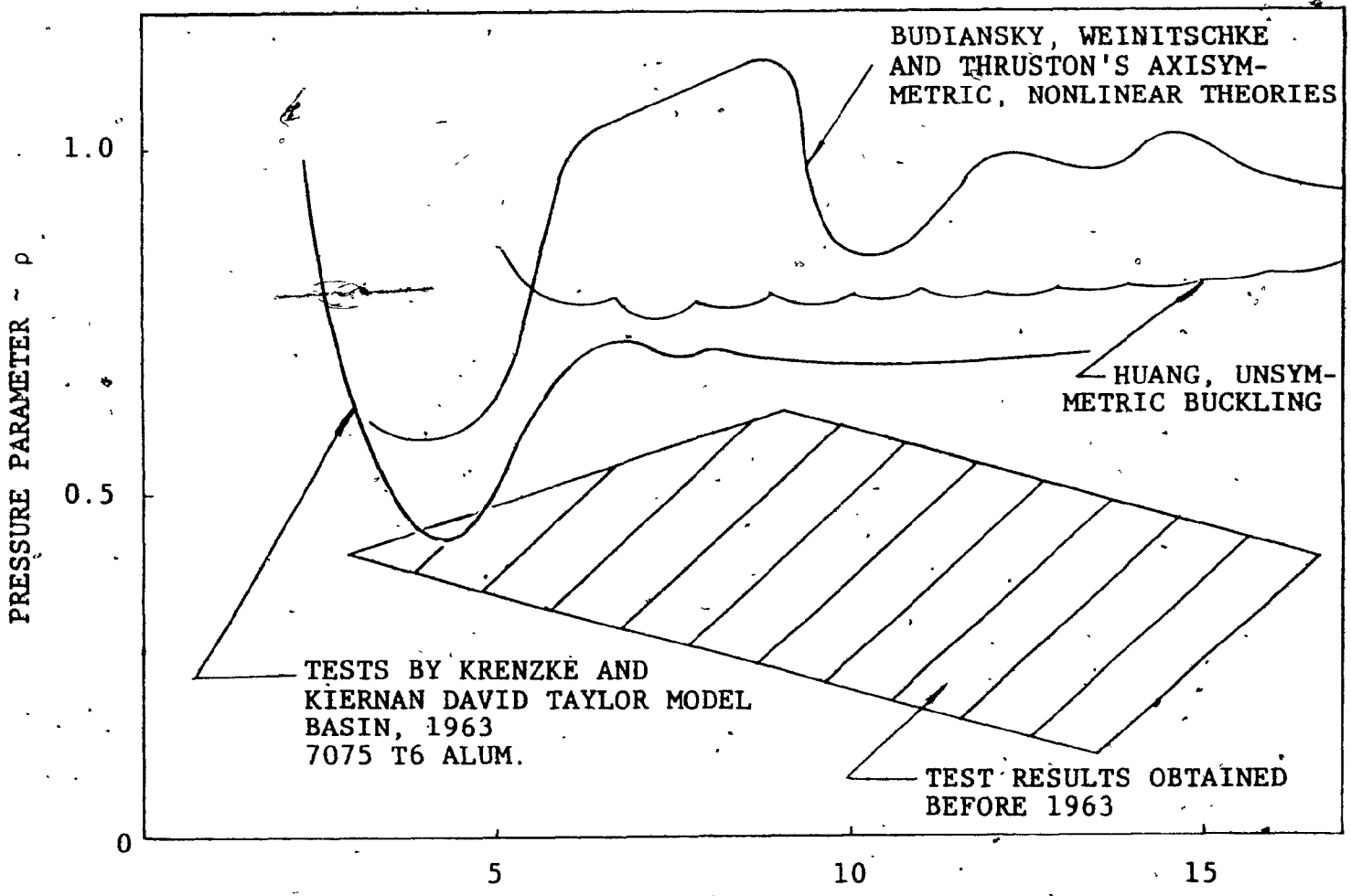

FIG. 2.2 Theoretical and Experimental Stability Curves

2.2 Strain-Displacement and Curvature Displacement Relations

The first step in the formulation of either the basic equilibrium relations of the potential energy expressions for spherical caps under external loads, is to determine the strain-displacement and the curvature-displacement relations.

The undeformed spherical shell shown in figure (2.3) is clamped along the edge. The independent variable "x" is the spherical angle measured from the centre of the cap. The dependent variables for the "equilibrium approach" are the horizontal and vertical components of displacement "u_a" and "w_a", measured at a point on the middle surface of the spherical cap. The symbol α denotes half the sustained spherical angle; "ε_x" and "ε_θ" denote the meridional and circumferential middle surface strains respectively; "κ_1" is the change in the curvature of the meridian during deformation and "κ_2" is that of the line of intersection of the middle surface of a plane normal to the undeformed meridian; "ds" and "ds_d" denote the undeformed and the deformed element respectively.

The meridional strain is then defined as

$$\varepsilon_x = \frac{d_{sd}}{ds} - 1 \qquad (2.1)$$

which can further be written as

$$\varepsilon_x = \left[\frac{(r_{,x} + u_{a,x})^2 + (z + w_{a,x})^2}{(r^2_{,x} + z^2_{,x})}\right]^{\frac{1}{2}} - 1 \qquad (2.2)$$

with the help of the geometrical relation shown in figure (2.4).

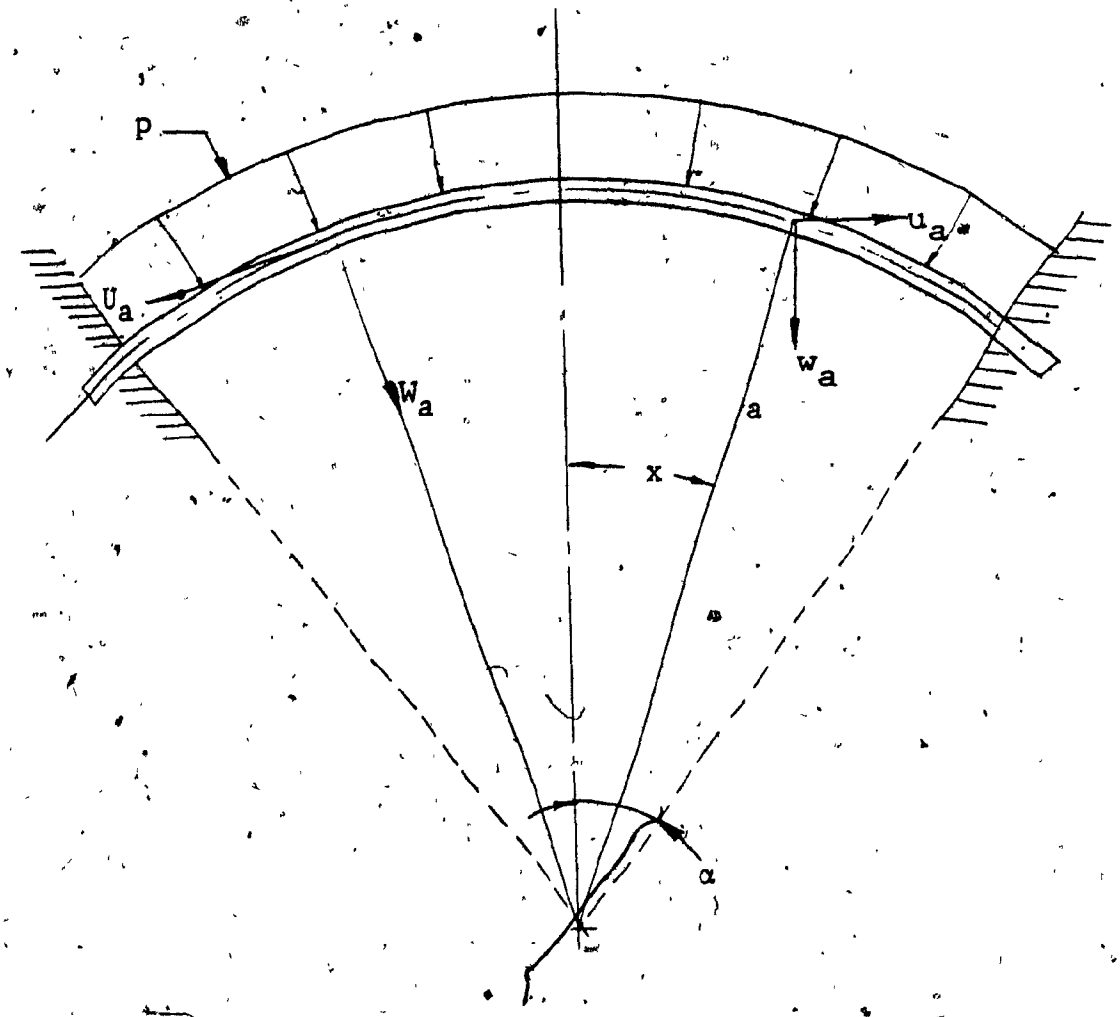

FIG. 2.3 Clamped Spherical Cap Displacements

NOTE: u_a, w_a Used in the Equilibrium Approach and
U_a and W_a Used in the Potential Energy Approach

In order to rewrite equation (2.2) in terms of the dependent and independent variables, the expressions under the square root are expanded by Taylor Series and the second order terms are approximated. Considering that $r = a \sin x$ and $z = a(1 - \cos x)$ and using the dimensionless values $u = u_a/a$ and $w = w_a/a$, it can be shown that the meridional strain is

$$\varepsilon_x = u_{,x} \cos x + w_{,x} \sin x + \frac{1}{2}(u_{,x}^2 + w_{,x}^2) \qquad (2.3)$$

the circumferential strain ε_θ can be written as

$$\varepsilon_\theta = \frac{(r + u_a)\, d_\theta}{r d_\theta} - 1 = \frac{u}{\sin x} \qquad (2.4)$$

Also from figure (2.4) the curvature of the meridian after deformation is defined by

$$\left.\begin{aligned} \frac{1}{R_1} &\equiv \frac{d\phi}{ds_d} = \phi_{,x} \frac{dx}{ds_d} \\ \text{where } \phi &= \tan^{-1}\left[\frac{z_{,x} + w_{a,x}}{r_{,x} + u_{a,x}}\right] \end{aligned}\right\} \qquad (2.5)$$

Differentiation of ϕ with respect to x gives,

$$\phi_{,x} = \left[\frac{(r_{,x} + u_{a,x})(z_{,xx} + w_{a,xx}) - (z_{,x} + w_{a,x})(r_{,xx} + u_{a,xx})}{(r_{,x} + u_{a,x})^2 + (z_{,x} + w_{a,x})^2}\right]$$

But

$$ds_d = (r_{,x} + u_{a,x})^2 dx^2 + (z_{,x} + w_{a,x})^2 dx^2$$

hence

$$\phi_{,x} = \left(\frac{dx}{ds_d}\right)^2 \left[(r_{,x} + u_{a,x})(z_{,xx} + w_{a,xx}) - (z_{,x} + w_{a,x})(r_{,xx} + u_{a,xx})\right] \qquad (2.6)$$

Further, as $ds = a\,dx$, then equation (2.1) can be expressed in the form,

$$\frac{dx}{ds_d} = \frac{1}{a(1 + \varepsilon_x)} \tag{2.7}$$

The curvature of the meridian after deformation can be expressed as given in equation (2.8) by combining equations (2.5) and (2.6).

$$\frac{1}{R_1} = \frac{(r_{,x} + u_{a,x})(z_{,xx} + w_{a,xx}) - (z_{,x} + w_{a,x})(r_{,xx} + u_{a,xx})}{a^3(1 + \varepsilon_x)^3} \tag{2.8}$$

"κ_1", the change of curvature of the meridian during deformation can be expressed as,

$$\kappa_1 \equiv \frac{1}{R_1} - \frac{1}{a} \tag{2.9}$$

Noting from figure (2.4) that

$$\left.\begin{aligned} (1 + \varepsilon_x)\cos\phi &= \cos x + u_{,x} \\ (1 + \varepsilon_x)\sin\phi &= \sin x + w_{,x} \end{aligned}\right\} \tag{2.10}$$

The middle surface strain may be assumed to be small compared to unity and therefore $\varepsilon_x \ll 1$. Hence, equations (2.3), (2.4) and (2.10) can be combined to express the change of curvature as

$$a\kappa_1 = (w_{,xx} - u_{,x})\cos\phi - (u_{,xx} + w_{,x})\sin\phi \tag{2.11}$$

Similarly, κ_2 can be expressed as

$$\kappa_2 = \frac{1}{R_2} - \frac{1}{a} \tag{2.12}$$

From figure (2.4) and equation (2.4), R_2 is given as

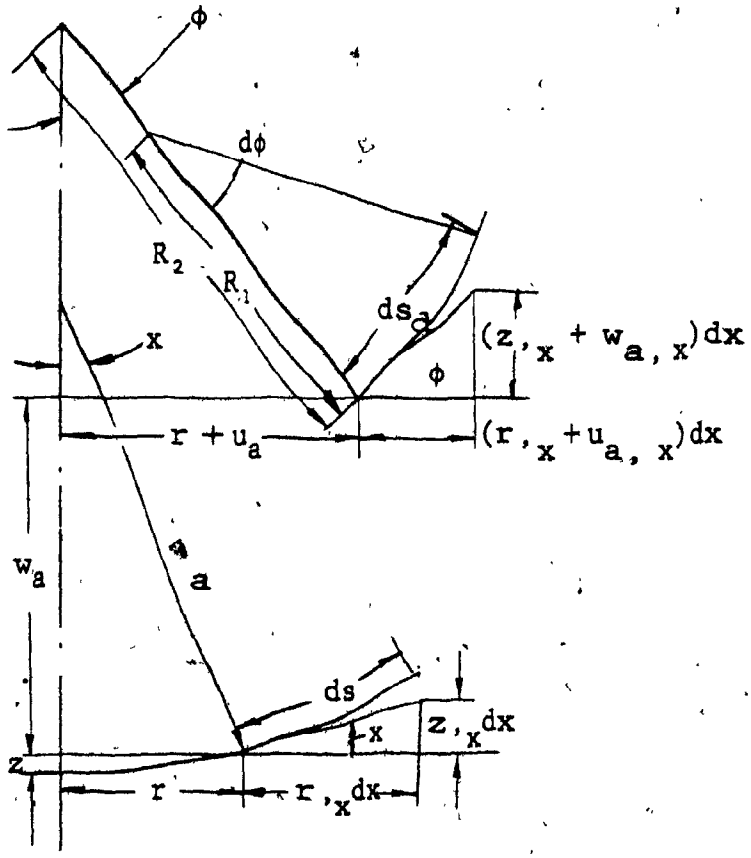

FIG. 2.4 Geometry of Undeformed and Deformed Element

$$\frac{1}{R_2} = \frac{\sin \phi}{r + u_a} = \frac{\sin \phi}{r(1 + \varepsilon_\theta)} \tag{2.13}$$

Substituting equation (2.13) into (2.12) and using the assumption $\varepsilon_\theta << 1$,

$$\kappa_2 = \frac{w_{,x}}{a \sin x} \tag{2.14}$$

Equations (2.3) and (2.4) define the strain-displacement relations and equations (2.11) and (2.14) the curvature-displacement relations which will be used in the derivation of the equilibrium equations and the potential energy expression for spherical shells.

2.3 Equations of Equilibrium

In the equilibrium approach [32] the force and moment equilibrium were derived by taking a deformed element of the middle surface under an external pressure "p" as shown in figure (2.5). The equation of equilibrium in the vertical direction is given by

$$[r(1+\varepsilon_\theta)(Q \cos \phi + N_x \sin \phi)]_{,x} + a\, r(1+\varepsilon_\theta)(1+\varepsilon_x)\, p \cos \phi = 0 \tag{2.15}$$

and in the direction along the tangent to the deformed meridian is given by

$$[r(1 + \varepsilon_\theta) N_x]_{,x} - a(1 + \varepsilon_x) N_\theta \cos \phi - r(1 + \varepsilon_\theta)\phi_{,x} Q = 0 \tag{2.16}$$

The moment equation is expressed by

$$[r(1 + \varepsilon_\theta)M_x]_{,x} - a(1+\varepsilon_x)\, M_\theta \cos \phi - a\, r(1 + \varepsilon_\theta)(1 + \varepsilon_x)\, Q = 0 \tag{2.17}$$

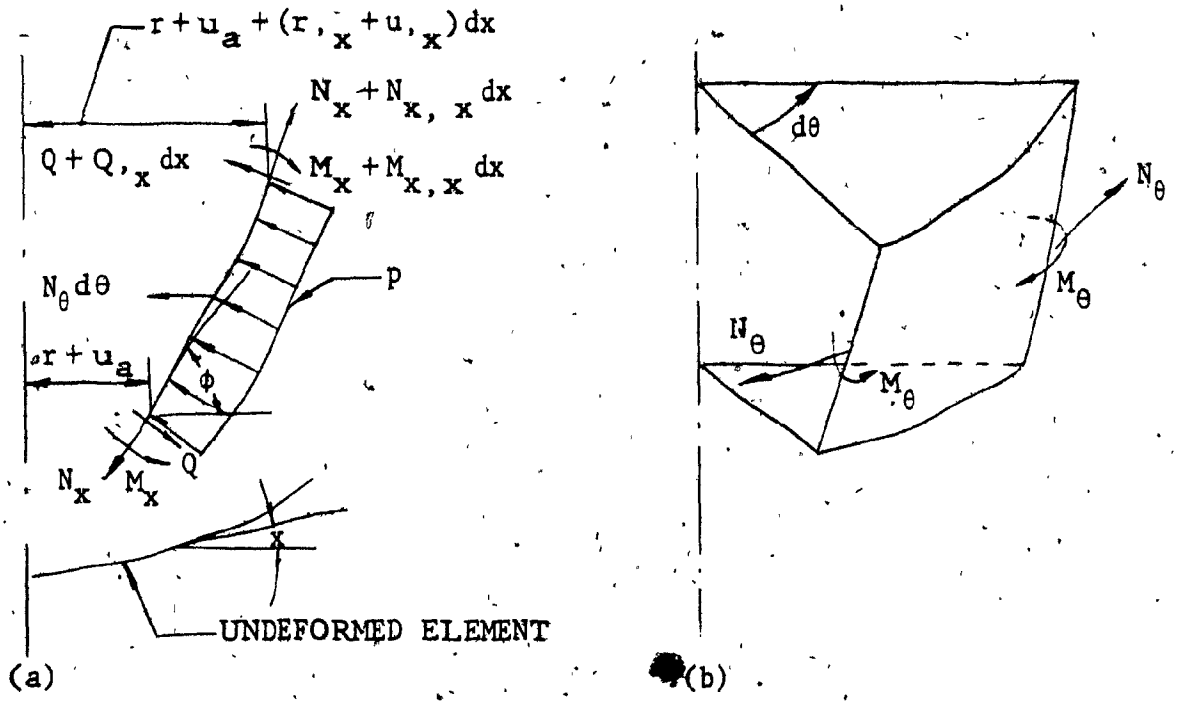

FIG. 2.5 (a) Deformed Meridian with Forces and Moments
(b) Deformed Element of Middle Surface with Circumferential Moments and Stress Resultants

where N_x is the meridional stress resultant, N_θ the circumferential stress resultant, Q the transverse shear, M_x the meridional moment resultant, M_θ the circumferential moment resultant and p the external pressure.

Derived by Bushnell [32] the above equations are valid for spherical shells of arbitrary depth with large strains, displacements and rotations.

In order to solve the above equations of equilibrium for strains smaller than unity, ϵ_x and ϵ_θ can be neglected with respect to "1". Equation (2.15) is, then, integrated to give

$$r(Q \cos \phi + N_x \sin \phi) = - a p \int r \cos \phi \, dx + c \qquad (2.18)$$

In equation (2.18), the integral part can further be reduced to a simplified form in the following steps

$$\int r \cos \phi \, dx = \int (a \sin x \cos x + a u_{,x} \sin x) \, dx$$

$$= u a \sin x + \int a \sin x \cos x \left(1 - \frac{u}{\sin x}\right) dx$$

$$= u a \sin x + \int a \sin x \cos x \, (1 - \epsilon_\theta) \, dx$$

$$\int r \cos \phi \, dx = u a \sin x + \frac{a}{2} \sin^2 x \qquad (2.19)$$

While arriving at equation (2.19), use has been made of equation (2.10) and the integration by parts.
The constant "c" in equation (2.18) is equated to zero due to the symmetry condition. Thus, equation (2.18) reduces to the form

$$r(Q \cos \phi + N_x \sin \phi)' = - \frac{pa^2}{2} \sin^2 x \qquad (2.20)$$

Equation (2.16) can be expressed by using relations (2.5 to 2.7)

$$r N_{x,x} + a \cos \phi (N_x - N_\theta) - r Q \frac{a}{R_1} = 0 \qquad (2.21)$$

and finally equation (2.17) can be expressed by

$$a Q = M_{x,x} + \frac{a}{r} \cos \phi (m_x - M_\theta) \qquad (2.22)$$

In obtaining equations (2.20 to 2.22) Bushnell [32] compared the order of magnitude of each term and neglected those comparatively very small. The three equilibrium equations (2.20 to 2.22) have seven unknowns, namely N_x, N_θ, M_x, M_θ, Q, ϕ and R; in order to solve these equations the following relations can be introduced.

For an elastic shell Hooke's law gives

$$N_x = \frac{Eh}{1 - \nu^2} (\varepsilon_x + \nu \varepsilon_\theta) \text{ and } N_\theta = \frac{Eh}{1 - \nu^2} (\varepsilon_\theta + \nu \varepsilon_x) \qquad (2.23)$$

where h is the shell thickness; E and ν are the Young's modulus and Poisson's ratio respectively.

Also the moments can be expressed in terms of the change in curvature κ_1 and κ_2 giving

$$M_x = - D(\kappa_1 + \nu \kappa_2) \text{ and } M_\theta = - D(\kappa_2 + \nu \kappa_1) \qquad (2.24)$$

where the flextural rigidity "D" is given by

$$D = Eh^3/12(1 - \nu^2) \qquad (2.25)$$

Now the number of unknowns is thirteen and is equal to the number of equations which are the strain-displacement

equations (2.3 and 2.4), the curvature-displacement equations (2.8, 2.9, 2.13 and 2.14), the equilibrium equations (2.20 to 2.22) and the four stress-strain relations (2.23 and 2.24). The solution for these unknowns cannot be completed without defining the boundary conditions for shells clamped along the edge

$$\left.\begin{aligned} & u|_{x=\alpha} = w|_{x=\alpha} = 0 \\ & (w_{,x}\cos x - u_{,x}\sin x)|_{x=\alpha} = 0 \end{aligned}\right\} \qquad (2.26)$$

Also from symmetry at x = 0

$$\left.\begin{aligned} & u|_{x=0} = w_{,x}|_{x=0} = Q|_{x=0} = 0 \\ & N_x|_{x=0} = N_\theta|_{x=0} \end{aligned}\right\} \qquad (2.27)$$

These general equations of equilibrium being difficult to solve were simplified by Bushnell [32].

2.4 Simplified Equations of Equilibrium

For shallow shells with a sustained angle "$\alpha << \pi$", and for small rotation "ϕ" equations (2.10) can be written as

$$\cos\phi = \cos x = 1 \text{ and } \sin\phi = \phi = x + w_{,x} \qquad (2.28)$$

The horizontal displacement "u" can be neglected compared to similar terms for the vertical displacement "w".

The simplified set of equations is according to Bushnell [32]:

$$(x\,M_x)_{,x} - M_\theta + a\,x\,N_x\,(x + w_{,x}) = -\frac{pa^2}{2}\,x^2 \qquad (2.29)$$

$$(x\, N_x)_{,x} = N_\theta \tag{2.30}$$

$$\left.\begin{aligned} \varepsilon_x &= u_{,x} + x\, w_{,x} + \tfrac{1}{2} w_{,x}^2 \\ \varepsilon_\theta &= u/x \end{aligned}\right\} \tag{2.31}$$

$$\kappa_1 = w_{,xx}/a \quad \text{and} \quad \kappa_2 = w_{,x}/ax \tag{2.32}$$

$$w_{,x}\Big|_{x=\alpha} = 0 \tag{2.33}$$

where equation (2.29) is that of the vertical equilibrium of forces from which "Q" has been eliminated by means of the moment equation (2.22); and equation (2.30) is that of the equilibrium in the direction of the deformed meridian.

2.4.1 Method of Solution for the Simplified Equations of Equilibrium

Introducing a parameter β to be the negative of the angle of rotation of the undeformed tangent during deformation, hence from equation (2.28)

$$w_{,x} \simeq -\beta \tag{2.34}$$

Also introducing the independent variable y and the dependent variable, f and g such that

$$y \equiv \frac{\pi}{\alpha} x \;; \quad f \equiv \frac{\pi}{\alpha} \beta \;; \quad \text{and} \quad g \equiv \left(\frac{\pi}{\alpha}\right)^3 u \tag{2.35}$$

Bushnell [32] used the above relations in conjunction with equations (2.23) and (2.28 through 2.34) to express the equilibrium equations in the vertical direction and along the tangent to the deformed meridian as follows

$$yf_{,yy} + f_{,y} - \frac{f}{y} + \frac{\lambda^4}{\pi^4}\frac{1}{1-\nu^2}\, y(y-f)\left(g_{,y} + \frac{\nu g}{y} - yf + \frac{1}{2}f^2\right) = - 2\frac{\lambda^2}{\pi^2}\rho y^2 \qquad (2.36)$$

$$yg_{,yy} + g_{,y} - \frac{g}{y} - (2-\nu)yf - y^2 f_{,y} + \frac{1-\nu}{2}f^2 + yff_{,y} = 0 \qquad (2.37)$$

where the geometric parameter λ is given by

$$\lambda^4 \equiv \left[12(1-\nu^2)\left(\frac{a}{h}\right)^2 \alpha^4\right] \qquad (2.38)$$

and the pressure parameter $\rho \equiv p/p_{cr}$, p_{cr} being the classical buckling pressure for a complete sphere

$$p_{cr} \equiv \frac{2E}{\sqrt{3(1-\nu^2)}}\left(\frac{h}{a}\right)^2 \qquad (2.39)$$

It should be noted here that Weinistchke [23], Budiansky [24] Thurston [25] and others have used the same geometric parameter "λ" in their works about the buckling of spherical caps.

Equations (2.36) and (2.37) represent a non-linear boundary value problem which can be solved by expanding $f(y)$ and $g(y)$ in finite trigonometric series while expanding y, y^2, y^3 and y^4 in a Fourier series in the interval $-\pi \leq y \leq \pi$, which corresponds to $-\alpha \leq x \leq \alpha$.

A computer program written by Hoff and Al [37], to obtain equations for the post-buckled equilibrium of an axially compressed cylindrical shell, was adapted by Bushnell [32] to the snap-through problem of a spherical cap. The new set of developed equations contains the free parameter λ and ρ.

2.4.2 Plotting of the Load-Deflection Curves

For every assigned value of the geometric parameter λ and of the pressure parameter ρ, a load displacement curve can be plotted against a normalized displaced volume "L" such that

$$L = \frac{L_a}{L_o} \tag{2.40}$$

where "L_a" is the volume of displacement during deformation and "L_o" the volume of displacement during snap through as shown in figure (2.6).

For small strains and shallow shells these volumes can be approximated as given below [22]:

$$\left.\begin{aligned} L_a &= \frac{2a^3\alpha^2}{\pi} \int_0^{\pi} wy \, dy \\ L_o &= \frac{\pi a^3 \alpha^4}{2} \end{aligned}\right\} \tag{2.41}$$

Figure (2.7) shows a typical plot of the pressure parameter ρ versus the normalized displaced volume "L" using a Fourier expansion with 5 terms, a geometric parameter $\lambda^2 = 45$ and a sustained spherical angle $\frac{\alpha}{\pi} = .1$.

As previously mentioned, only the stable portions of the curve can be plotted by using the equilibrium method. It should also be noted that this method fails to give adequate results for large values of the geometric parameter λ^2.

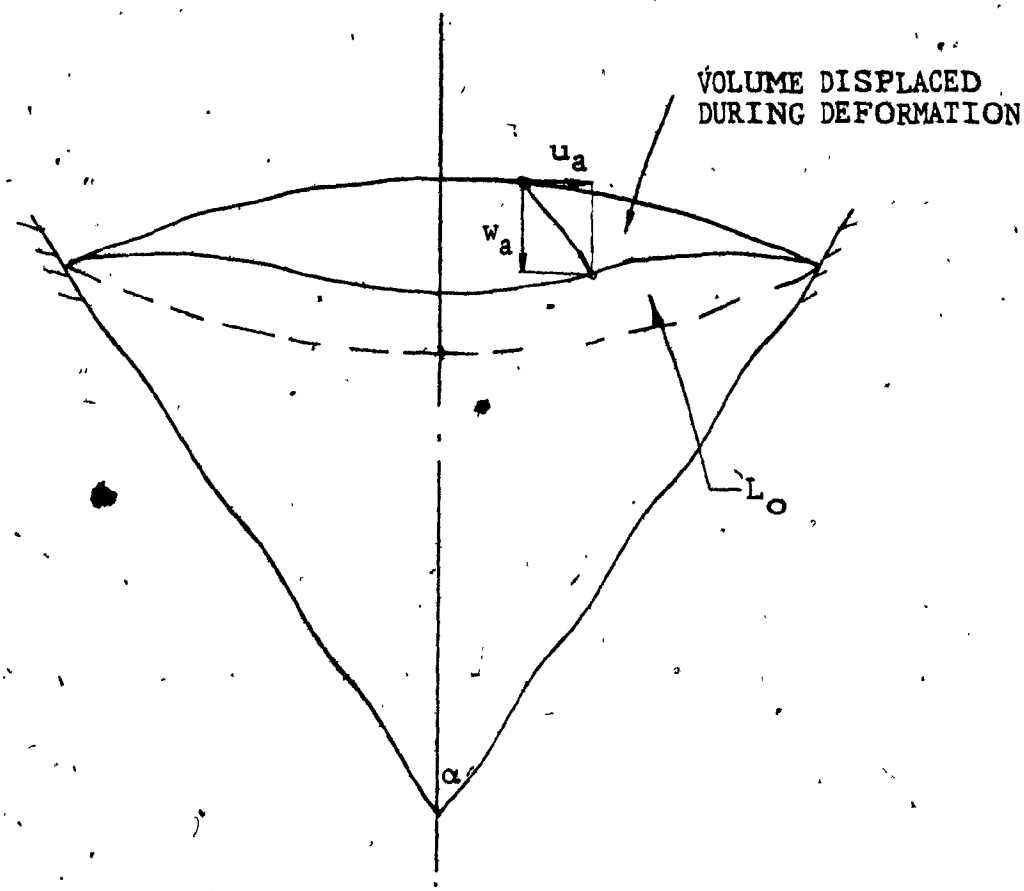

FIG. 2.6 Volume, L_a, Displaced During Deformation and "Snap-Through" Volume, L_o

2.5 Potential Energy Approach

The potential energy approach can be used for determining the unstable part of the load-displacement graph derived in section (2.3). It can also be used for determining the effect of imperfection on the load-deflection curves and for extending the solution of the load-displacement curves to values of the geometric parameter λ^2 in excess of 100. The dependent variables shown in figure (2.3) can be defined by U_a the tangential displacement and W_a the normal displacement, to the undeformed shell, hence:

$$\left.\begin{aligned} U_a &= u_a \cos x + w_a \sin x \\ W_a &= w_a \cos x - u_a \sin x \end{aligned}\right\} \qquad (2.42)$$

Bushnell also introduced the following identities:

$$\left.\begin{aligned} T &\equiv \frac{1}{a}\,[U_{a,x} - W_a] \\ S &\equiv \frac{1}{a}\,[W_{a,x} + U_a] \end{aligned}\right\} \qquad (2.43)$$

Then expressions (2.3), (2.4), (2.11) and (2.14) can be written in terms of U_a, W_a, T and S as

$$\left.\begin{aligned} \varepsilon_x &= T + \frac{1}{2}(T^2 + S^2) \\ \varepsilon_\theta &= \frac{1}{a}[U_a \cot\frac{\alpha}{\pi} y - W_a] \end{aligned}\right\} \qquad (2.44)$$

$$\left.\begin{aligned} a\kappa_1 &= [S_{,x}(1 + T) - S\,T_{,x}] \\ a\kappa_2 &= [S \cot\frac{\alpha}{\pi} y + T] \end{aligned}\right\} \qquad (2.45)$$

Defining the tangential and normal displacements to the undeformed meridian of the spherical shell in a dimensionless form:

$$U \equiv \left(\frac{\pi}{\alpha}\right)^3 \frac{U_a}{a} \quad \text{and} \quad W \equiv \left(\frac{\pi}{\alpha}\right)^2 \frac{W_a}{a} \tag{2.46}$$

and using equations (2.35) and (2.46), relations (2.43) and (2.44) can be written as:

$$\left.\begin{aligned} T &= \left(\frac{\alpha}{\pi}\right)^3 U_{,y} - \left(\frac{\alpha}{\pi}\right)^2 W \\ S &= \left(\frac{\alpha}{\pi}\right)^2 W_{,y} - \left(\frac{\alpha}{\pi}\right)^3 U \end{aligned}\right\} \tag{2.47}$$

$$\varepsilon_x = \left(\frac{\alpha}{\pi}\right)^2 \left[U_{,y} - W + \frac{1}{2} W_{,y}^2\right] + \frac{1}{2}\left(\frac{\alpha}{\pi}\right)^4 \left[(U_{,y} - W)^2 + 2W_{,y} U\right] + \frac{1}{2}\left(\frac{\alpha}{\pi}\right)^6 U^2 \tag{2.48}$$

$$\varepsilon_\theta = \left(\frac{\alpha}{\pi}\right)^3 U \cot \frac{\alpha}{\pi} y - \left(\frac{\alpha}{\pi}\right)^2 W \tag{2.49}$$

The approximate curvature-displacement relations (2.32) can also be written as

$$a\kappa_1 = W_{,yy} \quad \text{and} \quad a\kappa_2 = \left(\frac{\alpha}{\pi}\right) W_{,y} \cot \frac{\alpha}{\pi} y. \tag{2.50}$$

2.5.1 Total Potential Energy of the Shell

$$V = V_m + V_b - V_p. \tag{2.51}$$

where the total potential energy "V" is the sum of 'V_m', the membrane strain energy, "V_b" the bending strain energy and "V_p" the work done by the external pressure.

Using the flextural rigidity "D" defined by relation (2.25) and assuming that ε_x, $\varepsilon_\theta \ll \frac{h^2}{12\,a^2}(\kappa_1, \kappa_2)$, Bushnell [32] derived the following potential energy expressions,

$$\left.\begin{aligned} V_m &= \frac{Eh\,a^2\,\alpha}{1-\nu^2}\int_0^{\pi}(\varepsilon_x^2+\varepsilon_\theta^2+2\nu\varepsilon_x\,\varepsilon_\theta)\sin\frac{\alpha}{\pi}y\,dy \\ V_b &= Da^2\,\alpha\int_0^{\pi}(\kappa_1^2+\kappa_2^2+2\nu\,\kappa_1\kappa_2)\sin\frac{\alpha}{\pi}y\,dy \\ V_p &= 2\,pa^3\,\frac{\alpha^3}{\pi^2}\int_0^{\pi}W\sin\frac{\alpha}{\pi}y\,dy \end{aligned}\right\} \qquad (2.52)$$

And, for small displacements of shallow spherical caps where the radial displacement W_a is of the order of the shell thickness h, Bushnell [32] wrote the strain-displacement relation (2.48)

$$\varepsilon_x = \left(\frac{\alpha}{\pi}\right)^2\left[U_{,y} - W + \frac{1}{2}W_{,y}^2\right]$$

as only the first term of equation (2.48) predominates.

Expressions (2.51) and (2.52) can be written in terms of the displacements U and W, in order to arrive at a solution in the form of a load deflection graph, giving,

$$K\left(\frac{\pi}{\alpha}\right)^5 V = Iv_m + Iv_b - Iv_p \qquad (2.54)$$

where

$$K = \frac{2\sqrt{(1-\nu^2)}\,h}{\sqrt{3}\,p_{cr}\,a^4\alpha}$$

$$\left.\begin{aligned} Iv_m = \int_0^{\pi}\Big[&\left(U_{,y} - W + \frac{1}{2}W_{,y}^2\right)^2 + \left(\frac{\alpha}{\pi}U\cot\frac{\alpha}{\pi}y - W\right)^2 \\ &+ 2\nu\Big[U_{,y} - W + \frac{1}{2}W_{,y}^2\Big)\left(\frac{\alpha}{\pi}U\cot\frac{\alpha}{\pi}y - W\right)\Big]\frac{\pi}{\alpha}\sin\frac{\alpha}{\pi}y\,dy \\ Iv_b = (1-\nu^2)\frac{\pi^4}{\lambda^4}\int_0^{\pi}&\left(W_{,yy}^2 + \left(\frac{\alpha}{\pi}\right)^2\cot^2\frac{\alpha}{\pi}y\,W_{,y}^2\right. \\ &\left. + 2\nu\frac{\alpha}{\pi}\cot\frac{\alpha}{\pi}y\,W_{,yy}\,W_{,y}\right)\frac{\pi}{\alpha}\sin\frac{\alpha}{\pi}y\,dy \end{aligned}\right\} \qquad (2.56)$$

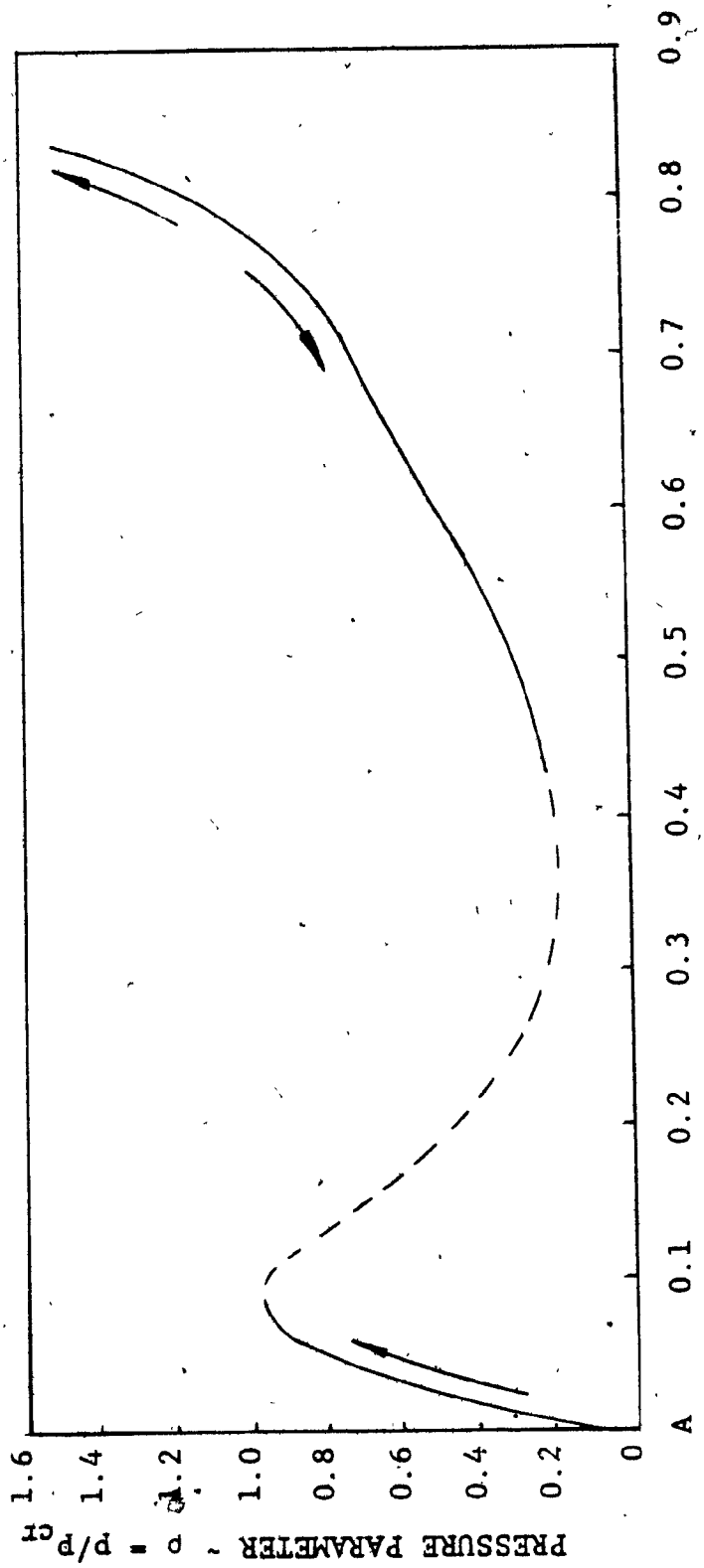

FIG. 2.7 Load-Deflection Curve for $\lambda^2 = 45$

$$Iv_p = -8\rho \frac{\pi^2}{\lambda^2} (1 - \nu^2) \int_0^{\pi} W \frac{\pi}{\alpha} \sin \frac{\alpha}{\pi} y \, dy \qquad (2.56) \text{ cont'd.}$$

2.5.2 Method of Solution of the Potential Energy Equation

In order to plot load-deflection curves similar to those drawn for the equilibrium approach, equation (2.54) should be solved for ρ against the normalized displacement volume L, for different values of the geometric parameter λ^2.

By minimizing the potential energy in expression (2.54) with respect to each of the undetermined coefficients, a set of non-linear algebraic equations are obtained. These algebraic equations can be solved by numerical analysis. Hoff [37], Madsen [38] and Bushnell [32] used Newton-Raphson iteration process to solve the above-mentioned non-linear equations.

Figures (2.7) through (2.11) show plots of the load-deflection curves for various values of λ^2. They also show the effect of imperfections of the type:

$$W_o = \delta(\cos y + 1) \qquad (2.57)$$

where a positive "δ" represents shells which are slightly flatter compared to perfectly spherical forms. Other cases of imperfections can be introduced and solved similarly by using the potential energy approach.

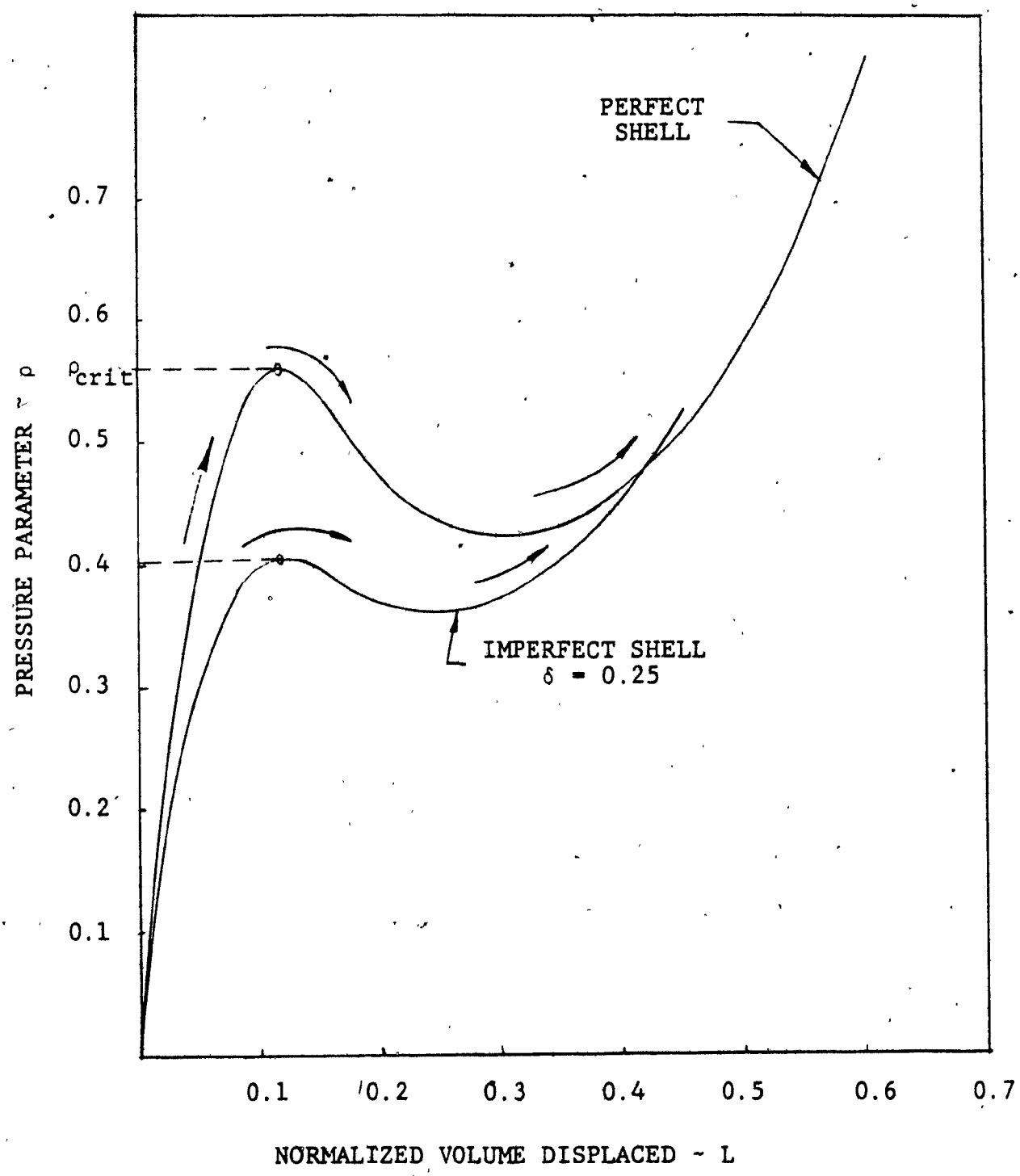

FIG. 2.8 Load-Deflection Curves for Perfect and Imperfect Shells for $\lambda^2 = 16$

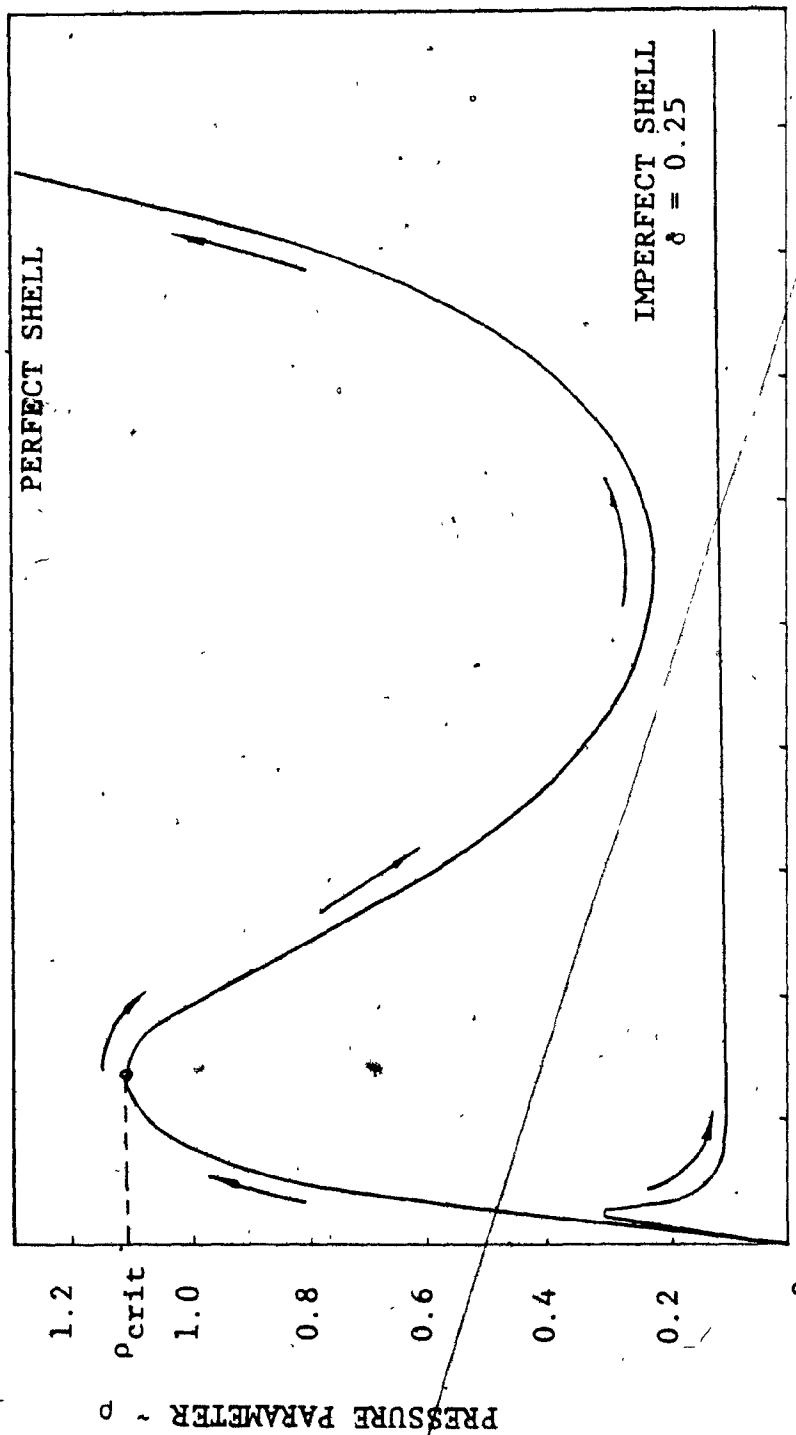

FIG. 2.9 Load-Deflection Curves for Perfect and Imperfect Shells, $\lambda^2 = 45$

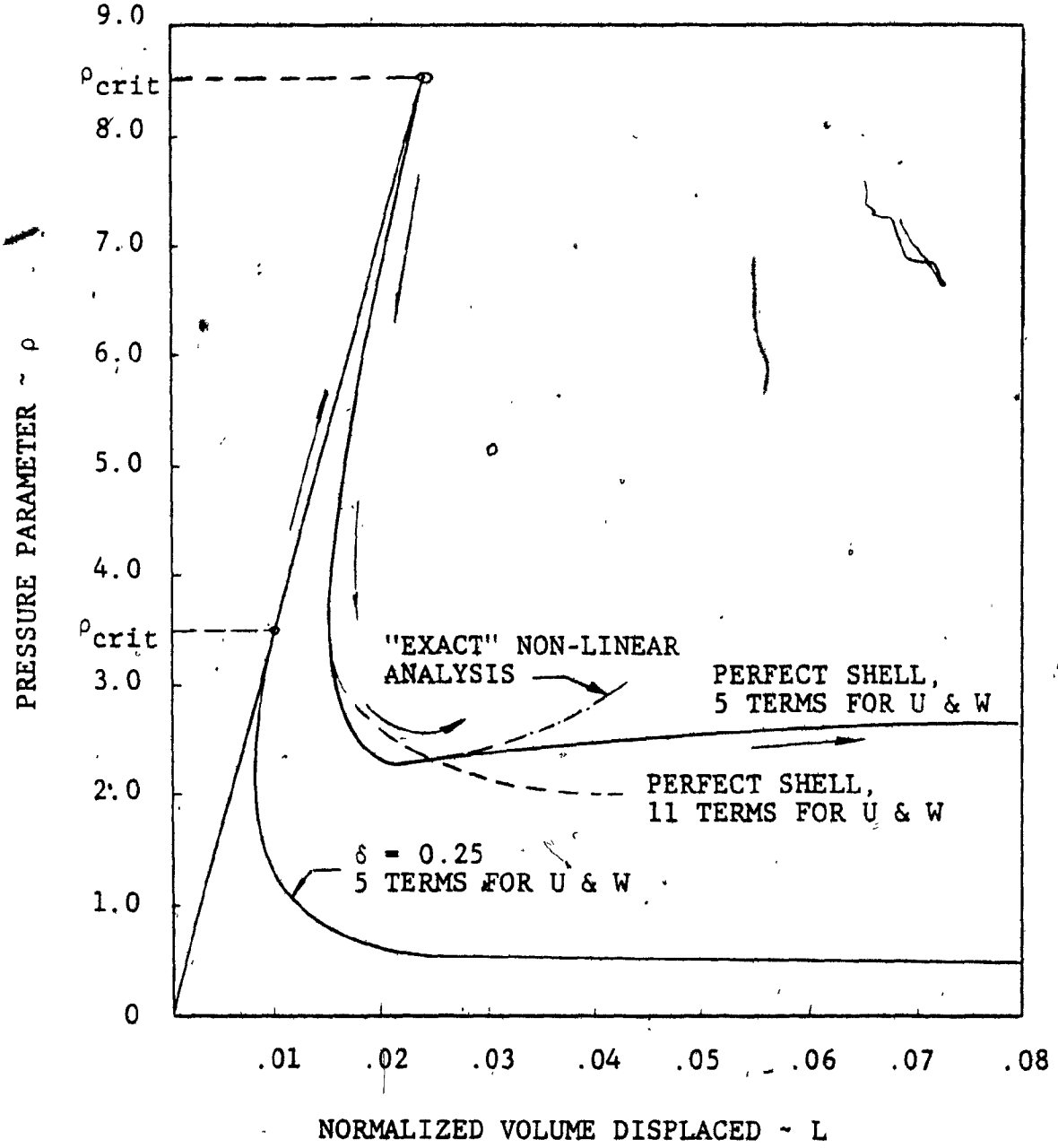

FIG. 2.10 Load-Deflection Curves for Perfect and Imperfect shells; $\lambda^2 = 100$

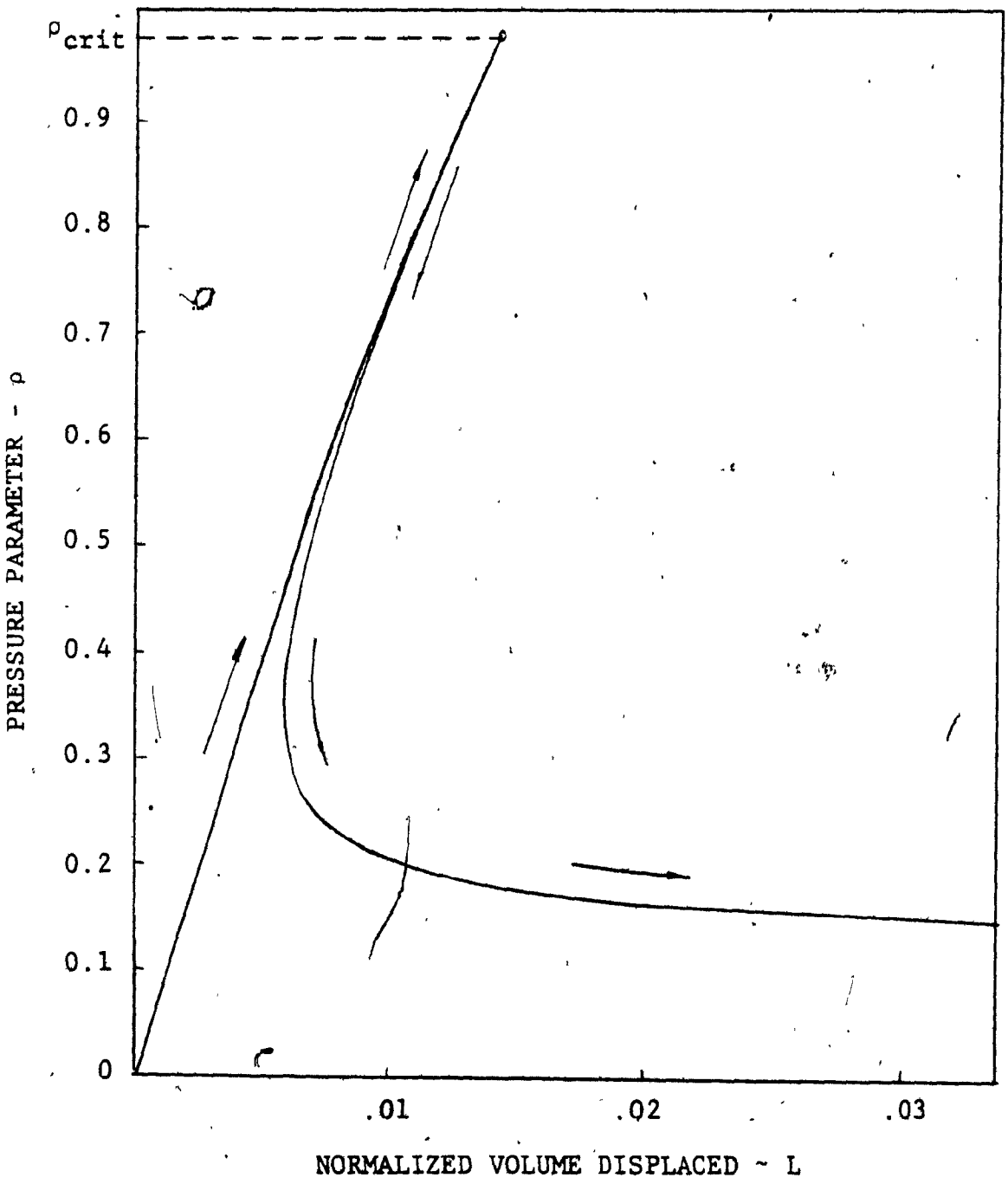

FIG. 2.11 Load-Deflection Curve for $\lambda^2 = 200$

2.6 Conclusion

The problem of axisymmetric deformation of a shallow elastic spherical shell subjected to external pressure has been approached from both the equilibrium and potential energy point of views. The latter leads to the determination of the unstable portions of the load-displacement curve, and also allows for the introduction of imperfections in the spherical caps.

Actual external loads affecting the excitation experienced by structures like spherical caps cannot be adequately described in terms of deterministic functions of time. These forces fluctuate in a random manner over a wide band of frequencies which can only be defined as stochastic functions of time in probabilistic terms. In the next chapter, the potential energy functions in the neighborhood of the stable and unstable states of the structure, will be used to derive analytical expressions for the probability of snap-buckling in a given time interval.

CHAPTER III

PROBABILITY OF FIRST SNAP-BUCKLING

Chapter III

PROBABILITY OF FIRST SNAP-BUCKLING

3.1 Introduction

As explained previously, two problems are associated with the equilibrium of shell-type structures when subjected to an external stochastic pressure load, namely snap-through and snap buckling. In the first case, the problem lies in the determination of the rate of diffusion of the probability density across the potential energy hump in a two-dimensional phase space. Figure (3.1a) shows a load deflection curve and figure (3.1b) a cross section of the potential energy surface. It may be noted that a single maximum corresponds to the unstable point "B". In the case of snap buckling, the problem involves evaluation of the rate of diffusion of the flux density along one of the principal directions in a four-dimensional phase space. As shown in figure (3.2b), the potential energy surface has a saddle point representing the unstable equilibrium state of the shell.

Due to the complexity of the potential energy equation (2.56), the analysis of the asymmetric dynamic instability will be first developed for cylindrical panels and then extended to spherical shells.

3.2 Potential Energy of Cylindrical Panels

Consider a cylindrical panel with radius a, thickness h, and a sustained angle α. Let the edge be hinged and be

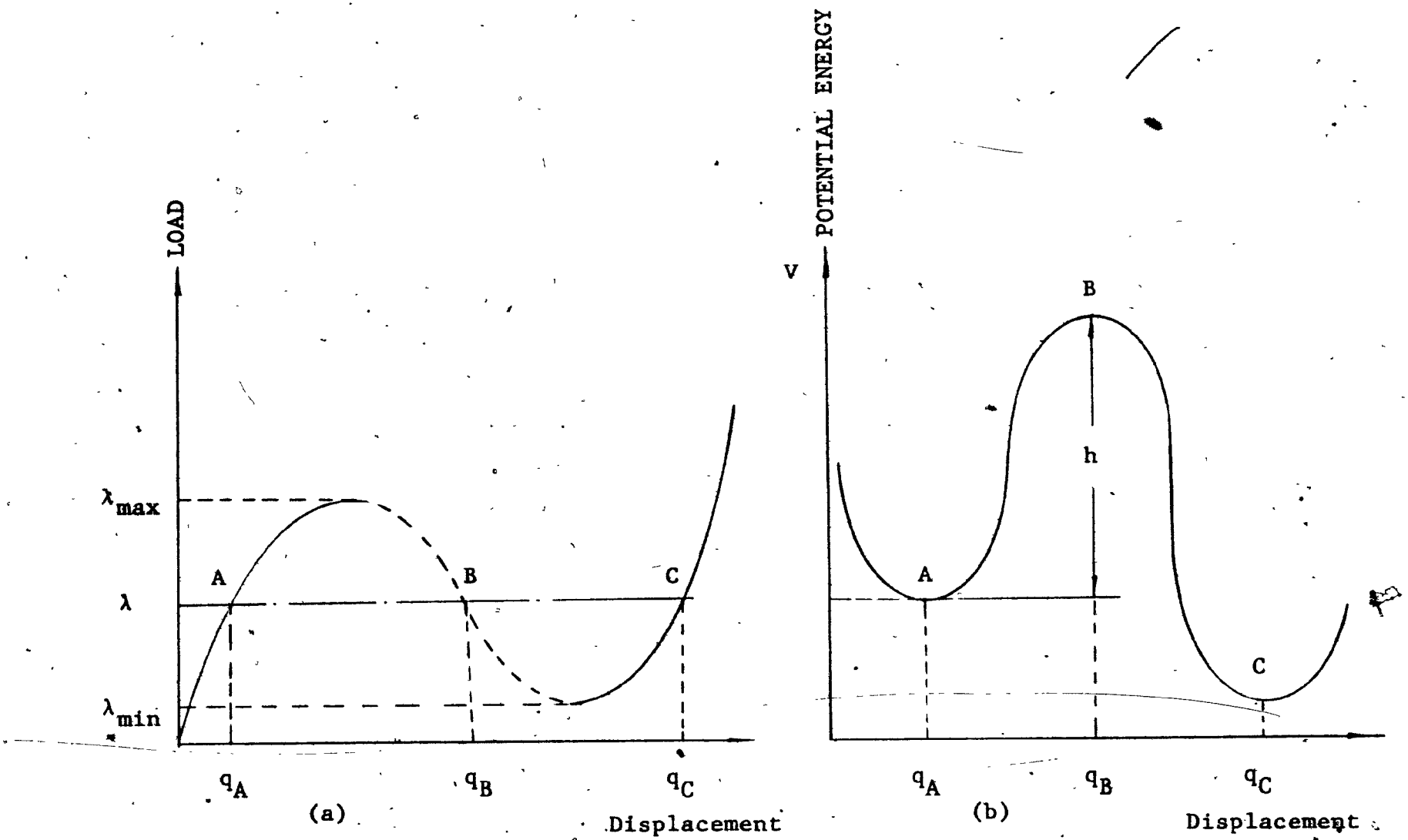

FIG. 3.1 Load-Deflection Curve and Section of Potential Energy Surface for Symmetric Snap-Through Problem

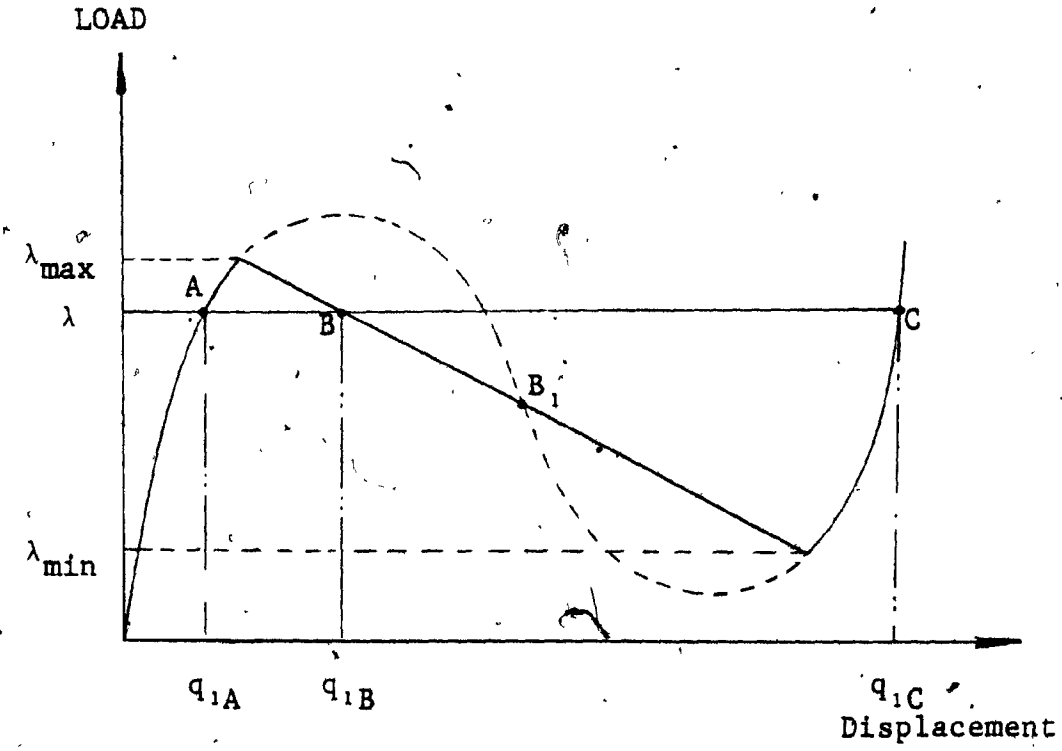

FIG. 3.2 (a) Load-Deflection Asymmetrical Case

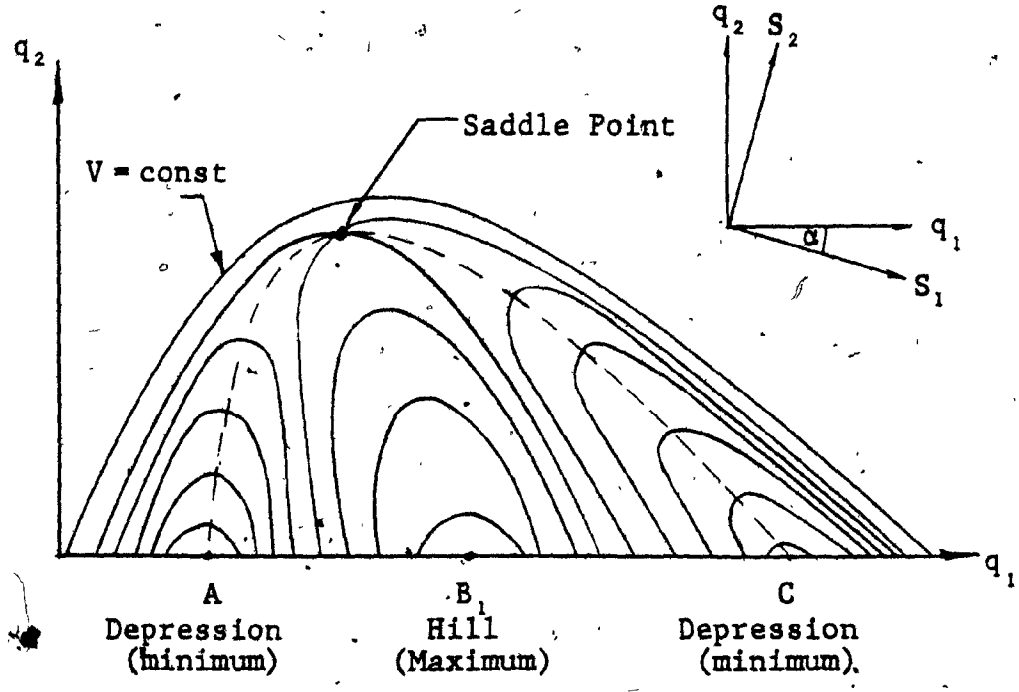

FIG. 3.2 (b) The Potential Energy System

immovable at $\phi = 0$ and $\phi = \alpha$.

The initial rise W_o is chosen such that along with a symmetric deformation an antisymmetric one is also excited under the action of the loads. With the coordinate axis shown in figure (3.3) the undeformed centreline of the panel is defined by $W_o(\phi)$. With the panel initially in a stable equilibrium state under a symmetrically distributed pressure of uniform intensity p, let it be subjected, at a time $t = 0$, to a random load of intensity $q(t)\ \sin(\frac{\pi\phi}{\alpha})$ having a zero mean value.

The deformed shape of the centreline of the rib at any time will be given by $W_1(\phi, t)$ and the deformation, as measured from the crown, at any other arbitrary point is

$$W(\phi, t) = W_o(\phi) - W_1(\phi, t) \tag{3.1}$$

$$= q_1 \sin(\frac{\pi\phi}{\alpha}) - q_2 \sin(\frac{2\pi\phi}{\alpha}) \tag{3.2}$$

Taking the coefficient of viscous damping β_o to be the same in both q_1 and q_2 modes of deformation, the equation of motion of the panel may be written using Lagrange's equation,

$$\frac{d}{dt}(\frac{\partial T}{\partial \dot{q}_i}) + \frac{\partial D_f}{\partial \dot{q}_i} - \frac{\partial T}{\partial q_i} + \frac{\partial V}{\partial q_i} = Q_i \tag{3.3}$$

where, $i = 1, 2$ represents the two degrees of freedom of the panel, T the kinetic energy of the system, D_f the dissipative function of the system, the total potential energy and Q_i the generalized forces corresponding to the applied loading on the panel; the quantities T, D_f, and V are evaluated as:

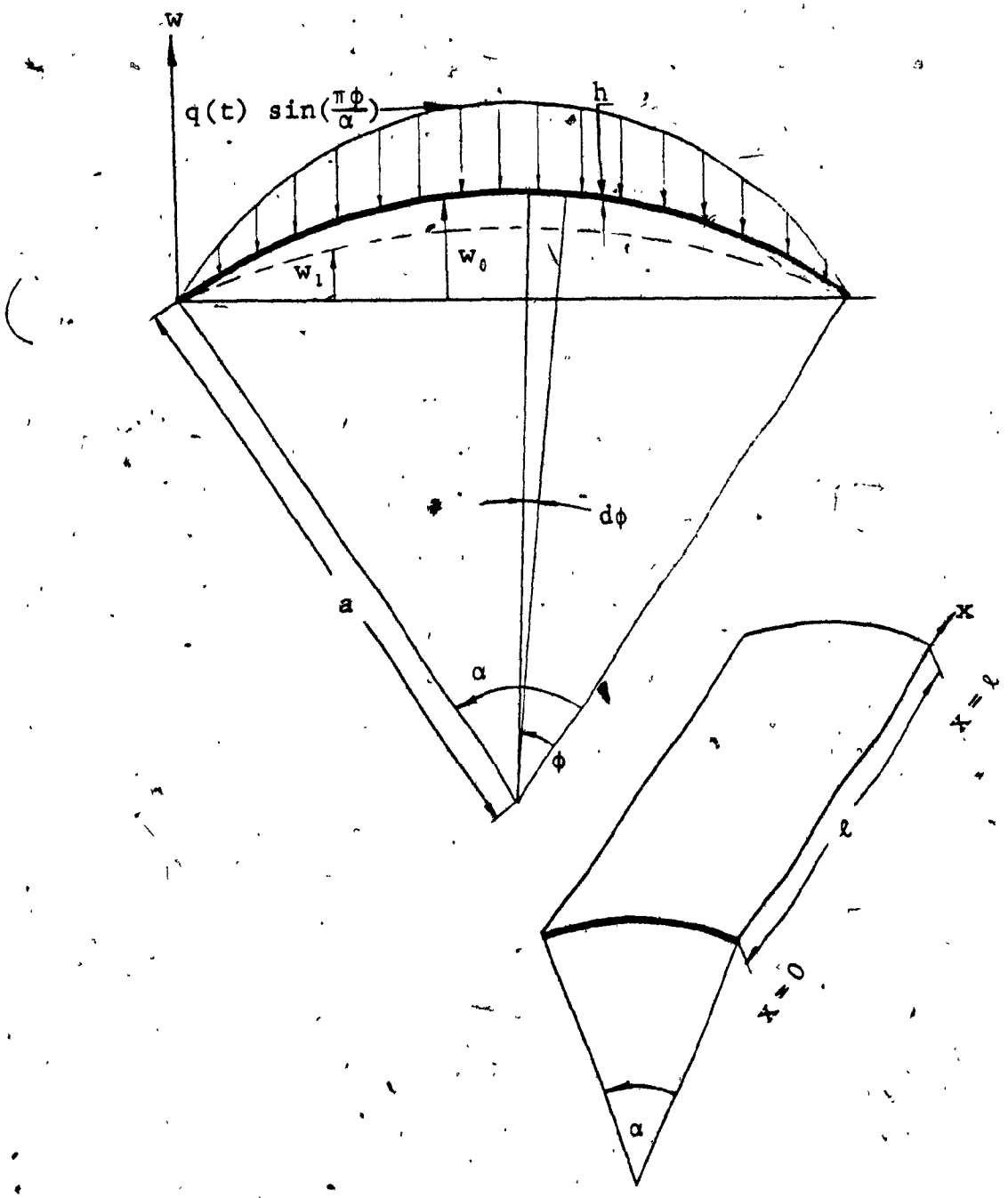

FIG. 3.3 Panel Geometry and Loading

$$T = \frac{\bar{\rho}h}{2} \int_0^{\alpha}\int_0^{\ell} \dot{W}^2 \, dx \, a \, d\phi$$

$$= \frac{\bar{\rho}ha\ell}{2} \int_0^{\alpha} (\dot{q}_1 \sin\frac{\pi\phi}{\alpha} - \dot{q}_2 \sin\frac{2\pi\phi}{\alpha})^2 \, d\phi$$

$$= \frac{\bar{\rho}ha\ell}{2}(\dot{q}_1^2 \, \frac{\alpha}{2} + \dot{q}_2^2 \, \frac{\alpha}{2})$$

as $m = \bar{\rho}ha\ell\alpha$

hence $$T = \frac{1}{4} \, m(\dot{q}_1^2 + \dot{q}_2^2) \qquad (3.4)$$

where m is the mass and $\bar{\rho}$ the density of the panel.

$$D_f = \frac{1}{4} \, \beta_0(\dot{q}_1^2 + \dot{q}_2^2) \qquad (3.5)$$

$$Q_1 = \frac{a\alpha}{2} \, q(t) \qquad (3.6)$$

$$Q_2 = 0 \qquad (3.7)$$

As in the case of spherical caps, the potential energy V of a cylindrical panel is determined from the strain energy V_m due to axial shortening, the strain energy V_b due to bending and the work done V_p by the external load $p \sin\frac{\pi\phi}{\alpha}$

$$V = V_m + V_b - V_p \qquad (3.8)$$

the various components of the potential energy are

$$V_m = \frac{D_f}{2} \int_\sigma \int_0^{\ell} \int_0^{\alpha} (\frac{12}{h^2} e^2) \, dx \, a d\phi$$

$$= \frac{D_f}{2} \, \frac{12}{h^2} \, \ell a \, \alpha e^2$$

$$= \frac{3\pi^4 \, D_f \, \ell}{2a^3 \, \alpha^3 \, h^2} [(\frac{1}{2}q_1^2 + 2q_2^2)^2 - \frac{4a\alpha^2}{\pi^3} q_1(q_1^2 + 4q_2^2)$$

$$+ \frac{16a^2 \, \alpha^4}{\pi^6} q_1^2] \qquad (3.9)$$

where e [40], the average strain due to axial shortening, is given by

$$e = \frac{\pi^2}{2a^2\alpha^2}\left(\frac{1}{2}q_1^2 + 2q_2^2\right) - \frac{2}{\alpha\pi}q_1 \tag{3.10}$$

$$V_b = \frac{D_f}{2}\int_0^{\ell}\int_0^{\alpha}\frac{1}{a^4}\left(\frac{\partial^2 W}{\partial\phi^2}\right)dx\ a\ d\phi$$

$$= \frac{D_f\,\ell a}{a^4}\int_0^{\alpha}\left(-\frac{\pi^2}{\alpha^2}q_1\sin\frac{\pi\phi}{\alpha} + \frac{4\pi^2}{\alpha^2}q_2\sin\frac{2\pi\phi}{\alpha}\right)^2 d\phi$$

leading to

$$V_b = \frac{3\pi^4 D_f\,\ell}{2a^3\alpha^3 h^2}\cdot\frac{h^2}{6}(q_1^2 + 16q_2^2) \tag{3.11}$$

$$V_p = \int_0^{\ell}\int_0^{\alpha}(p + q(t))\sin\frac{\pi\phi}{\alpha}\,W\,dx\ a\,d\phi$$

$$= p\,\ell\,a\int_0^{\alpha}\left(q_1\sin^2\frac{\pi\phi}{\alpha} - q_2\sin\frac{\pi\phi}{\alpha}\sin\frac{2\pi\phi}{\alpha}\right)d\phi + \text{const.}$$

which may be calculated as

$$V_p = \frac{3\pi^4 D_f\,\ell}{2a^3\alpha^3 h^2}\left(\frac{a^4\alpha^4 ph^2}{3\pi^5 D_f}\right)q_1 + \text{const.} \tag{3.12}$$

The total potential energy, equation (3.8), can now be written

$$V = \frac{3\pi^4 D_f\,\ell}{2a^3\alpha^3 h^2}\left[\left(\frac{1}{2}q_1^2 + 2q_2^2\right)^2 - \frac{4a\alpha^2}{\pi^3}q_1(q_1^2 + 4q_2^2)\right.$$
$$\left. + \left(\frac{16a^2\alpha^4}{\pi^6} + \frac{h^2}{6}\right)q_1^2 + \frac{8}{3}h^2q_2^2 - \frac{a^4\alpha^4 ph^2}{3\pi^5 D_f}q_1\right] + \text{const.} \tag{3.13}$$

Define a strength parameter $K' = \frac{3\pi^4 D_f\,\ell}{2a^3\alpha^3 h^2}$ and static load parameter $\lambda' = \frac{a^4\alpha^4 ph^2}{3\pi^5 D_f}$ in equation (3.13)

$$V = K'\left[\left(\frac{1}{2}q_1^2 + 2q_2^2\right)^2 - \frac{4a\alpha^2}{\pi^3}q_1(q_1^2 + 4q_2^2) + \left(\frac{16a^2\alpha^4}{\pi^6} + \frac{h^2}{6}\right)q_1^2\right.$$
$$\left. + \frac{8}{3}h^2q_2^2 - \lambda' q_1\right] + \text{const.} \tag{3.14}$$

3.3 Lagrange's Equation of Motion

On substitution in each term of Lagrange's equation of motion (3.3) with the corresponding terms in expressions (3.4, 3.5, 3.6, 3.7) and (3.14) for i = 1 and 2, one can arrive at

$$\left.\begin{aligned} \frac{m}{2}\ddot{q}_1 + \frac{\beta_o}{2}\dot{q}_1 + \frac{\partial V}{\partial q_1} &= Q_1 \\ \frac{m}{2}\ddot{q}_2 + \frac{\beta_o}{2}\dot{q}_2 + \frac{\partial V}{\partial q_2} &= 0 \end{aligned}\right\} \qquad (3.15)$$

Introducing the viscous damping parameter $\bar{\beta} = \frac{\beta_o}{m}$ and the generalized force function $\xi(t) = \frac{2Q_i}{m}$ in equation (3.15), yields

$$\left.\begin{aligned} \ddot{q}_1 + \bar{\beta}\dot{q}_1 + \frac{2}{m}\frac{\partial V}{\partial q_1} &= \xi(t) \\ \ddot{q}_2 + \bar{\beta}\dot{q}_2 + \frac{2}{m}\frac{\partial V}{\partial q_2} &= 0 \end{aligned}\right\} \qquad (3.16)$$

where $\frac{\partial V}{\partial q_1}$ and $\frac{\partial V}{\partial q_2}$ are the partial derivatives of equation (3.14) given by

$$\frac{\partial V}{\partial q_1} = K'\left[q_1^3 + 4q_1q_2^2 - \frac{16a\,\alpha^2}{\pi^3}q_2^2 - \frac{12a\,\alpha^2}{\pi^3}q_1^2 + \frac{32a^2\,\alpha^4}{\pi^6}q_1 + \frac{h^2}{3}q_1 - \lambda'\right] \qquad (3.17)$$

$$\frac{\partial V}{\partial q_2} = K'\left[16q_2^3 + \left(4q_1^2 - \frac{32a\,\alpha^2}{\pi^3}q_1 + \frac{16h^2}{3}\right)q_2\right] \qquad (3.18)$$

3.4 The Load-Deflection Curves

For any given value of the static parameter λ' the equilibrium configurations of the system are given by

$$\frac{\partial V}{\partial q_1} = 0 \qquad \text{and} \qquad \frac{\partial V}{\partial q_2} = 0 \tag{3.19}$$

or

$$q_1^3 + 4q_1 q_2^2 - \frac{16a\alpha^2}{\pi^3} q_2^2 - \frac{12a\alpha^2}{\pi^3} q_1^2 + \left(\frac{32a^2\alpha^4}{\pi^6} + \frac{h^2}{3}\right) q_1 - \lambda' = 0 \tag{3.20}$$

$$16\, q_2^3 + \left(4q_1^2 - \frac{32a\alpha^2}{\pi^3} q_1 + \frac{16h^2}{3}\right) q_2 = 0 \tag{3.21}$$

The roots of equations (3.20) and (3.21) describe the load-deflection curve of the panel shown in figure (3.4). The points A, B, B_1 and C correspond to the four equilibrium configurations of the panel. "A" is the initial stable state, "B_1" the unstable state of equilibrium and "C" the final stable buckled state of equilibrium associated with the symmetric deformation node q_1 only. The other unstable state of equilibrium of the structure, configuration "B", is associated with both the symmetric and the antisymmetric modes of deformation. The equilibrium configurations corresponding to A($q_1 = q_{1A}$ and $q_2 = 0$) and C($q_1 = q_{1C}$ and $q_2 = 0$) are determined by the roots of equation (3.20) after setting $q_2 = 0$ while the configuration of B($q_1 = q_{1B}$ and $q_2 = q_{2B}$) is given by a solution satisfying both equations (3.20) and (3.21).

3.5 Probability of First Snap-Buckling

In order to determine the probability of the first snap-buckling Sankar and Ariaratnam [2, 3] used the Fokker-Plank's equation technique. The state of the panel at any instant

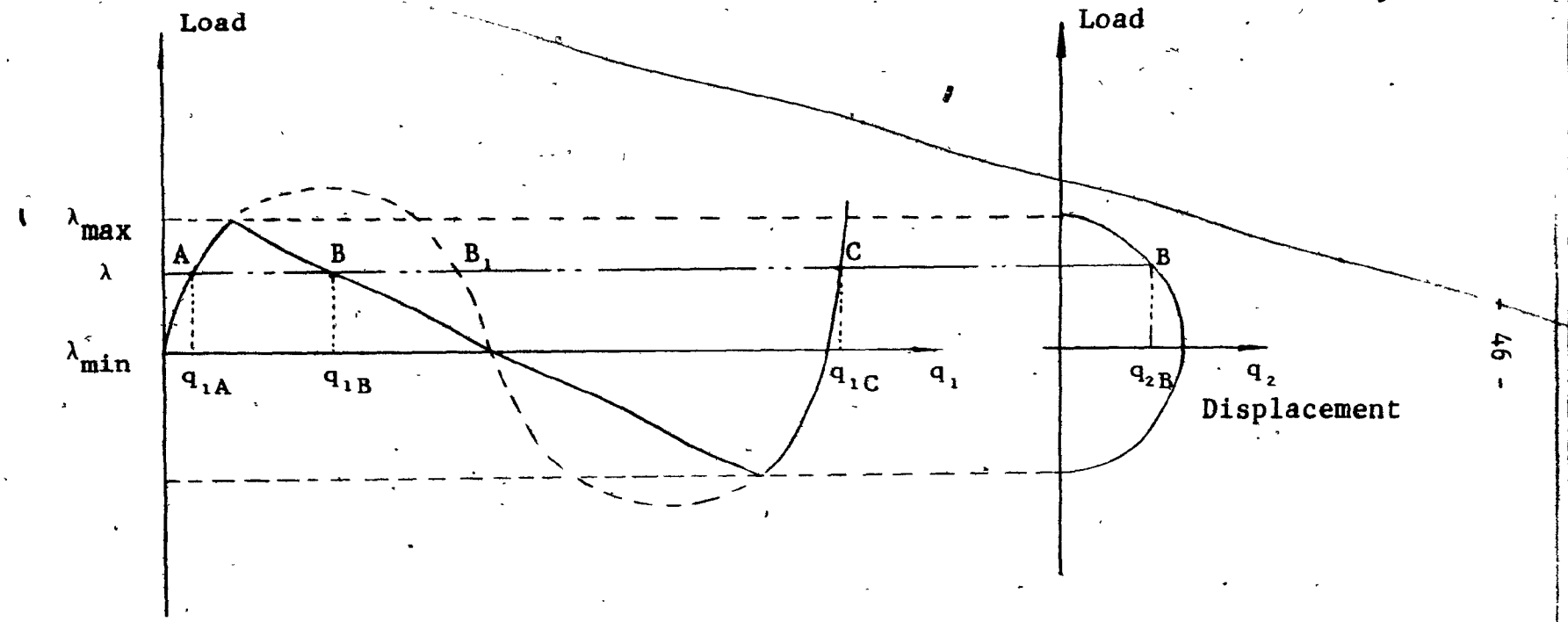

FIG. 3.4 Load-Deflection Characteristics

is defined by the phase variables $(q_1, q_2, \dot{q}_1, \dot{q}_2, t)$ under the applied stochastic load $\xi(t)$. When the first probability density $p(q_1, q_2, \dot{q}_1, \dot{q}_2, t)$ of the vector random process is known, the probability of first snap buckling is then derived as [3]:

$$P_T = \frac{T}{2\pi} \cos^2\alpha \left[\frac{(V_{11})_A}{-(\bar{V}_{11})_B}\right]^{\frac{1}{2}} \{ [\frac{\bar{\beta}^2}{4} - (\bar{V}_{11})_B]^{\frac{1}{2}} - \frac{\bar{\beta}}{2} \} \exp \left[\frac{-\bar{\beta}H}{D_f}\right] \qquad (3.22)$$

Introducing the non-dimensional parameters $\zeta_i = \frac{q_i}{h}$, expression (3.14) becomes

$$\left.\begin{aligned} V(\zeta_1, \zeta_2, \lambda) = \frac{2\bar{K}}{mh^2} \Big[&(\tfrac{1}{2}\zeta_1^2 + 2\zeta_2^2) - B\zeta_1(\zeta_1^2 + 4\zeta_2^2) \\ &+ C\zeta_1^2 + \tfrac{8}{3}\zeta_2^2 - \lambda\zeta_1 \Big] + \text{const.} \end{aligned}\right\} \qquad (3.23)$$

$$\left.\begin{aligned} \text{where} \quad \bar{K} = \frac{mh^2}{2}(K'h^4), \quad B = \frac{4a\alpha^2}{\pi^3 h} \\ C = \frac{16a^2\alpha^4}{\pi^6 h^2} + \frac{1}{6}, \quad \lambda = \frac{\lambda'}{h^3} \end{aligned}\right\} \qquad (3.24)$$

setting $\frac{\partial V}{\partial \zeta_1} = 0$ and $\frac{\partial V}{\partial \zeta_2} = 0$, the equilibrium configuration ζ_A, ζ_B and ζ_C of the panel are given by the roots of the following equations,

$$\left.\begin{aligned} &\zeta_1^3 + (\zeta_1 - B)(4\zeta_2^2) - 3B\zeta_1^2 + 2C\zeta_1 - \lambda = 0 \\ &4\zeta_2^2 + (\zeta_1^2 - 2B\zeta_1 + \tfrac{4}{3}) = 0 \end{aligned}\right\} \qquad (3.25)$$

For the stable equilibrium configuration, positions A and C of the panel, shown in figure (3.2) the antisymmetric deformation is given by $\zeta_2 = 0$. Using this in the first of equations (3.25), gives the solutions.

$$\left.\begin{aligned} \zeta_{1A} &= B - 2\left(\frac{3B^2 - 2C}{3}\right)^{\frac{1}{2}} \cos\left(\frac{\pi - \theta}{3}\right) \\ \zeta_{1C} &= B + 2\left(\frac{3B^2 - 2C}{3}\right)^{\frac{1}{2}} \cos\left(\frac{\theta}{3}\right) \end{aligned}\right\} \tag{3.26}$$

where θ is the angle of transformation given by

$$\cos\theta = \frac{2B(C - B^2) - \lambda}{2}\left(\frac{3}{3B^2 - 2C}\right)^{3/2}$$

The unstable configuration of B is given by a solution satisfying both equations (3.25). That is,

$$\zeta_{1B}^3 + (\zeta_{1B} - B)(-\zeta_{1B}^2 + 2\zeta_{1B} - \tfrac{4}{3}) - 3B\zeta_{1B}^2 + 2C\zeta_{1B} - \lambda = 0 \tag{3.27}$$

with solution

$$\left.\begin{aligned} \zeta_{1B} &= \frac{4B}{3} - \lambda \\ \zeta_{2B} &= \frac{1}{2}(2B\zeta_{1B} - \zeta_{1B}^2 - \tfrac{4}{3})^{\frac{1}{2}} \end{aligned}\right\} \tag{3.28}$$

$\zeta_{2B} = 0$ determines the limits of the static load parameter λ_{min} and λ_{max}.

$$\zeta_{1B} = B \pm \sqrt{B^2 - \tfrac{4}{3}}$$

$$\text{hence } \lambda_{min},\ \lambda_{max} = \tfrac{1}{3}B \mp \sqrt{B^2 - \tfrac{4}{3}} \tag{3.29}$$

For the roots to be real and distinct the mean static load parameter must be such that

$$\tfrac{1}{3}B - \sqrt{B^2 - \tfrac{4}{3}} < \lambda < \tfrac{1}{3}B + \sqrt{B^2 - \tfrac{4}{3}} \tag{3.30}$$

The natural frequency of the panel for a zero initial curvature in its fundamental mode ζ_1, after setting $\zeta_2 = 0$, is

given by $\omega_1 = \left(\frac{2\bar{K}}{mh^2}\right)^{\frac{1}{2}}$ which when introduced in the energy equation (3.23) gives,

$$V(\zeta_1, \zeta_2, \lambda) = \omega_1^2 [(\tfrac{1}{2}\zeta_1^2 + 2\zeta_2^2)^2 - B\zeta_1(\zeta_1^2 + 4\zeta_2^2) + C\zeta_1^2 + \tfrac{8}{3}\zeta_2^2 - \lambda\zeta_1] + \text{const} \tag{3.31}$$

3.6 Probability of Snap-Buckling: General Case

$(V_{11})_A = \frac{\partial^2 V}{\partial \zeta_1^2}$ evaluated at $\zeta_1 = \zeta_{1A}$ and $\zeta_2 = 0$

$$(V_{11})_A = \omega_1^2 (3\zeta_{1A}^2 - 6B\zeta_{1A} + 2C) \tag{3.32}$$

$(\bar{V}_{11})_B = \frac{\partial^2 \bar{V}}{\partial \bar{\zeta}_2^2}$ evaluated at $\bar{\zeta}_1 = \bar{\zeta}_{1B}$ and $\bar{\zeta}_2 = \bar{\zeta}_{2B}$

$$(\bar{V}_{11})_B = \frac{(V_{11})_B + (V_{22})_B}{2} - \frac{1}{2}\left[(V_{11})_B - (V_{22})_B \right]^2 + 4(V_{12})_B^2 \Big\}^{\frac{1}{2}} \tag{3.33}$$

As computed by Sankar and Ariaratnam [3] using Mohr's circle technique.

Now each term of equation (3.33) can be evaluated:

$$\left.\begin{aligned} (V_{11})_B &= \frac{\partial^2 V}{\partial \zeta_1^2} \\ &= \omega_1^2 (2\zeta_{1B}^2 - 4B\zeta_{1B} + 2C - \tfrac{4}{3}) \\ (V_{22})_B &= \frac{\partial^2 V}{\partial \zeta_2^2} \\ &= \omega_1^2 (-8\zeta_{1B}^2 + 16\, B\zeta_{1B} - \tfrac{32}{3}) \end{aligned}\right\} \tag{3.34}$$

$$(V_{12})_B = \frac{\partial^2 V}{\partial \zeta_1 \partial \zeta_2}$$

$$(V_{12})_B = \omega_1^2\{4[-\zeta^4_{1B} + 4B\zeta^3_{1B} - (4B^2 + B + \tfrac{4}{3})\zeta^2_{1B} + 2B(\tfrac{4}{3} + B^2)\zeta_{1B} - \tfrac{4}{3}B^2]^{\frac{1}{2}}\} \quad \text{(3.34) cont'd.}$$

Let

$$L = \frac{(V_{11})_B + (V_{22})_B}{2}$$

$$= \omega_1^2(-3\zeta^2_{1B} + 6B\zeta_{1B} +$$

$$M = \frac{(V_{11})_B - (V_{22})_B}{2}$$

$$= \omega_1^2(5\zeta^2_{1B} - 10B\zeta_{1B} + C + \tfrac{14}{3}) \quad (3.35)$$

$$N = (V_{12})_B$$

$$= 4\omega_1^2[-\zeta^4_{1B} + 4B\zeta^3_{1B} - (4B^2 + B + \tfrac{4}{3})\zeta^2_{1B} + 2B(B^2 + \tfrac{4}{3})\zeta_{1B} - \tfrac{4}{3}B^2]^{\frac{1}{2}}$$

Equation (3.33) can then be written in terms of equations (3.35),

$$(\overline{V}_{11})_B = [L - (M^2 + N^2)^{\frac{1}{2}}] \quad (3.36)$$

the probability of first snapping of the panel in a time interval T can now be written using equations (3.22) and (3.36):

$$P_T = \frac{T}{2\pi}\cos^2\alpha\left[\frac{(V_{11})_A}{-L + (M^2 + N^2)^{\frac{1}{2}}}\right]^{\frac{1}{2}}\{(\frac{\overline{\beta}^2}{4} - [L - (M^2 + N^2)^{\frac{1}{2}}])^{\frac{1}{2}} - \frac{\overline{\beta}}{2}\}\exp(\frac{-\overline{\beta}H}{D_f}) \quad (3.37)$$

where α is the angle of transformation given by

$$\tan 2\alpha = \frac{2(V_{12})_B}{(V_{11})_B - (V_{22})_B} = \frac{N}{M}$$

The height H of the potential barrier is calculated by Sankar and Ariaratnam [3] for similar problems to be

$$H = V(\zeta_{1B}, \zeta_{2B}) - V(\zeta_{1A}, 0) \tag{3.38}$$

from equation (3.23), the expressions giving the height of the potential barrier for a cylindrical panel are written

$$\left.\begin{aligned} V(\zeta_{1B}, \zeta_{2B}) &= \omega_1^2 h^2 (-\tfrac{1}{2}\zeta_{1B}^2 + (\tfrac{4}{3}B - \lambda)\zeta_{1B} - \tfrac{4}{9}) \\ V(\zeta_{1A}, 0) &= \omega_1^2 h^2 (\tfrac{1}{4}\zeta_{1A}^4 - B\zeta_{1A}^3 + C\zeta_{1A}^2 - \lambda\zeta_{1A}) \end{aligned}\right\} \tag{3.39}$$

Further introduce a nondimensional damping coefficient γ such that $\bar{\beta} = 2\gamma\omega_1$. Then the probability of first snapping of the panel in a given time is:

$$P_T = \frac{T\cos^2\alpha}{\tau_1}\left[\frac{3\zeta_{1A}^2 - 6B\zeta_{1A} + 2C}{-L + (M^2+N^2)^{\frac{1}{2}}}\right]^{\frac{1}{2}} \{[\gamma^2 - L + (M^2+N^2)^{\frac{1}{2}}]^{\frac{1}{2}} - \gamma\} \exp\left(\frac{2\gamma\omega_1 H}{D_f}\right) \tag{3.40}$$

where τ_1 is the period for the fundamental oscillation ω_1.

3.7 Symmetric Snap-Through

The deformed shape of the centreline of the panel can be found by setting $q_2 = 0$ in expression (3.2):

$$w(\phi, t) = q_1 \sin\left(\frac{\pi\phi}{\alpha}\right) \tag{3.41}$$

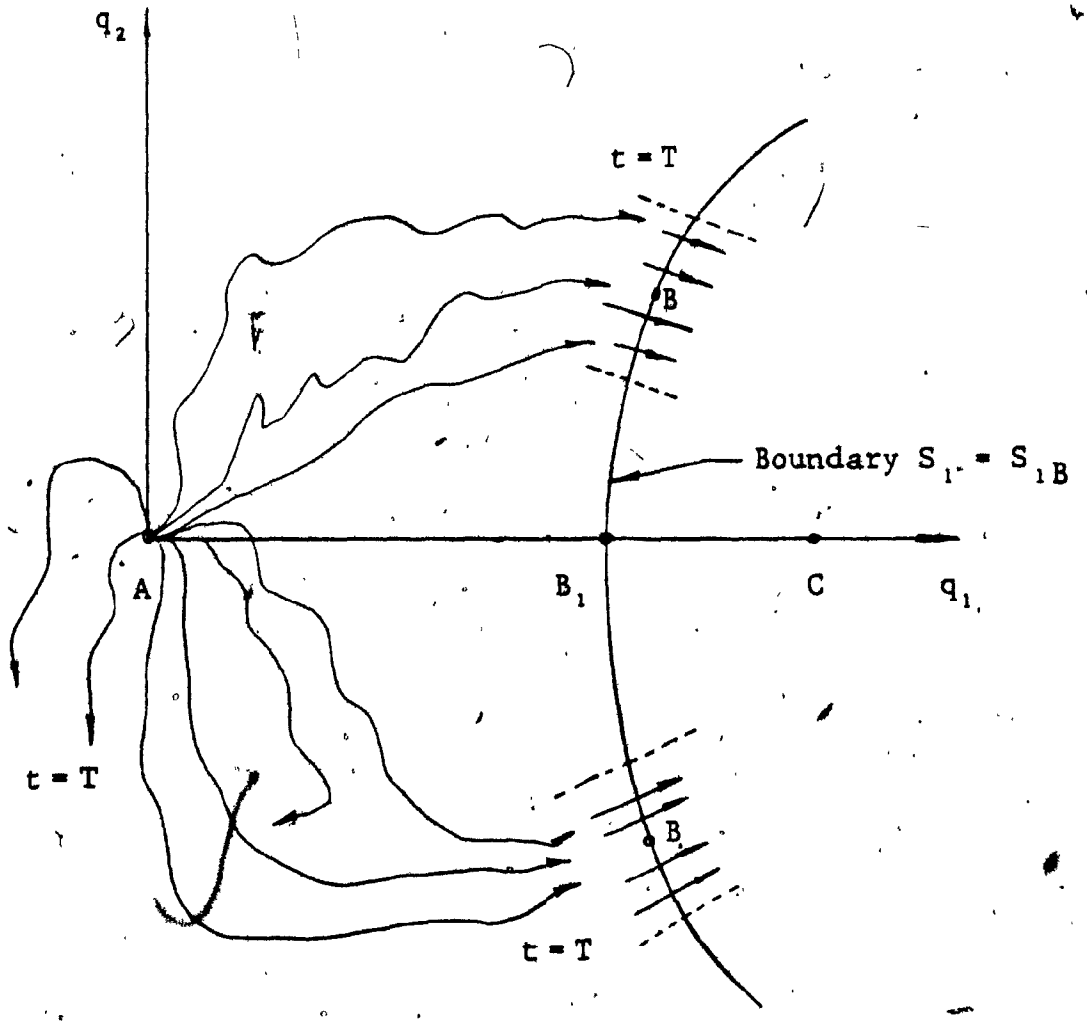

FIG. 3.5. Random Motion of Phase Points (Particles).

The kinetic and potential energy are from equations (3.4) and (3.14)

$$\left.\begin{aligned} T &= \frac{1}{4} m\dot{q}_1^{\,2} \\ V &= K'\left[\frac{1}{4} q_1^{\,4} - \frac{4a\,\alpha^2}{\pi^3} q_1^{\,3} + \left(\frac{16a^2\alpha^2}{\pi^6} + \frac{h^2}{6}\right) q_1^{\,2} - \lambda \cdot q_1\right] + \text{const} \end{aligned}\right\} \quad (3.42)$$

the equilibrium equations are from equation (3.25)

$$\zeta_1^{\,3} - 3B\zeta_1^{\,2} + 2C\zeta_1 - \lambda = 0 \quad (3.43)$$

The stable equilibrium configuration A and C of the panel and the unstable configuration B are given by the solution of equation (3.43):

$$\left.\begin{aligned} \zeta_{1A} &= B - 2\left(\frac{3B^2 - 2C}{3}\right)^{\frac{1}{2}} \cos\left(\frac{\pi - \theta}{3}\right) \\ \zeta_{1B} &= B - 2\left(\frac{3B^2 - 2C}{3}\right)^{\frac{1}{2}} \cos\left(\frac{\pi + \theta}{3}\right) \\ \zeta_{1C} &= B + 2\left(\frac{3B^2 - 2C}{3}\right)^{\frac{1}{2}} \cos\left(\frac{\theta}{3}\right) \\ \text{where } \cos\theta &= \frac{2B(C - B^2) - \lambda}{2}\left(\frac{3}{3B^2 - 2C}\right)^{3/2} \end{aligned}\right\} \quad (3.44)$$

the limits for λ are given by setting $\cos\theta = \pm 1$

$$2B(C - B^2) + 2\left(B^2 - \frac{2}{3}C\right)^{3/2} > \lambda > 2B(C - B^2) - 2\left(B^2 - \frac{2}{3}C\right)^{3/2} \quad (3.45)$$

From equation (3.31) the potential energy is:

$$V(\zeta, \lambda) = \omega_1^{\,2}\left(\frac{1}{4}\zeta_1^{\,4} - B\zeta_1^{\,2} + C\zeta_1^{\,2} - \lambda\zeta_1\right) + \text{const} \quad (3.46)$$

$$\text{hence } \frac{\partial^2 V}{\partial \zeta^2} = \omega_1^{\,2}\left(3\zeta_1^{\,2} - 6B\zeta_1 + 2C\right) \quad (3.47)$$

3.8 Height of the Potential Barrier

$$H = V(q_B) - V(q_A) \tag{3.48}$$

$$= [V]_A^B - \frac{h\zeta}{4}[\frac{\partial V}{\partial q}]_A^B$$

where

$$[V]_A^B = [\int \frac{\partial V}{\partial \zeta}\, d\zeta]_A^B \equiv h[\int \frac{\partial V}{\partial q}\, d\zeta]_A^B$$

$$= \omega_1^2 h^2 [\frac{\zeta^4}{4} - B\zeta^3 + C\zeta^2 - \lambda\zeta]_A^B$$

$$\frac{h}{4}[\frac{\partial V}{\partial q}]_B^A = \omega_1^2 h^2 [\frac{\zeta^4}{4} - \frac{3}{4} B\zeta^3 + \frac{1}{2}\zeta^2 - \frac{\lambda}{4}\zeta]_A^B$$

hence $$H = \omega_1^2 h^2 [-\frac{1}{4} B\zeta^3 + \frac{1}{2}\zeta^2 - \frac{3}{4}\lambda\zeta]_A^B \tag{3.49}$$

P_T, the probability of first snap buckling of the panel at a given time interval T is written from equations (3.22, 3.46, 3.47) and (3.49);

$$P_T = \frac{T\omega_1}{2\pi} \left(\frac{3\zeta_A^2 - 6B\zeta_A + 2C}{3\zeta_B^2 + 6B\zeta_B + 2C}\right)^{\frac{1}{2}} [(\gamma - 3\zeta_B^2 + 6B\zeta_B - 2C)^{\frac{1}{2}} - \gamma]$$

$$\exp\left(\frac{-2\gamma\omega_1 H}{D}\right) \tag{3.50}$$

3.9 Conclusion

The probability of failure by instability in a given time time interval has been evaluated for a given panel of known properties and random load intensity. The applicability of the results were extended to include any general case of buckling where both symmetric and asymmetric deformations

are involved due to the degree of shallowness of the panel curvature.

Numerical application and results will be discussed in the next chapter. This will lead to determination of the fields where this theory could be applied and extended to the design stage in the form of charts and plots.

CHAPTER IV

APPLICATIONS

Chapter IV

APPLICATIONS

4.1 Introduction

The dynamic buckling of low cylindrical space panels of known geometry and elasticity when subjected to distributed surface pressure was investigated in the previous chapters where only the general theory was presented for deriving "P_T" the probability of failure of cylindrical panels. Two types of snap-through buckling were discussed based on the initial curvature of the panel. Numerical results for a specimen panel of assumed dimensions will be presented as an application of the probability of first snap buckling to illustrate the solution of equations (3.40 and 3.50).

The non-linear equations of motion of the panel can be solved for a stationary wide band Gaussian random loading through locally stationary solutions of the associated Fokker-Planck equations by approximating the response to a Markov process in the phase plane.

4.2 Application of the Analysis

A cylindrical panel of a given geometry is considered under an assumed random loading of intensity S in order to illustrate the application of the analysis developed in the previous chapters. By defining a fundamental period τ_1 of the panel vibrations the time for failure T is conveniently

taken as a multiple of τ_1. P_T, the failure probability is computed for different values of the damping ratio γ/γ_c, γ_c being the critical damping of the system, and for various mean dead loads λ which are expressed as ratio λ/λ_{max} with λ_{max} being the maximum admissible static critical load on the panel surface.

Consider first the symmetric snap-through problem (Figure 4.1) where $\zeta_2 = 0$. For various damping values of γ/γ_c the variation of the logarithm of P_T, the probability of first failure given by equation (3.50) is plotted in figure (4.2) against the nondimensional load ratio λ/λ_{max}. To excite only a symmetric displacement the panel under study has a value h/a of 1/3000 which indicates the degree of shallowness of the structure. It also has an initial deflection ratio h/y_o equal to unity. As for the random load intensity S is taken to be $0.1\ \omega_1^3 h^2$ and a time ratio of $T/\tau_1 = 3600$ is taken as the basis for computing the probability of failure.

Figure (4.2) shows that the probability of failure increases at a rapid rate as the mean dead load "λ" approaches λ_{max} the critical load, and this probability decreases as γ/γ_c increases. Further, the probability of failure is extremely sensitive, for a given structure, to the ratio of the height of the potential barrier to the impressed random loading intensity H/S. Which means that the structural system may be in a stable equilibrium under the mean dead load "λ" applied, however the possiblity of failure by buckling

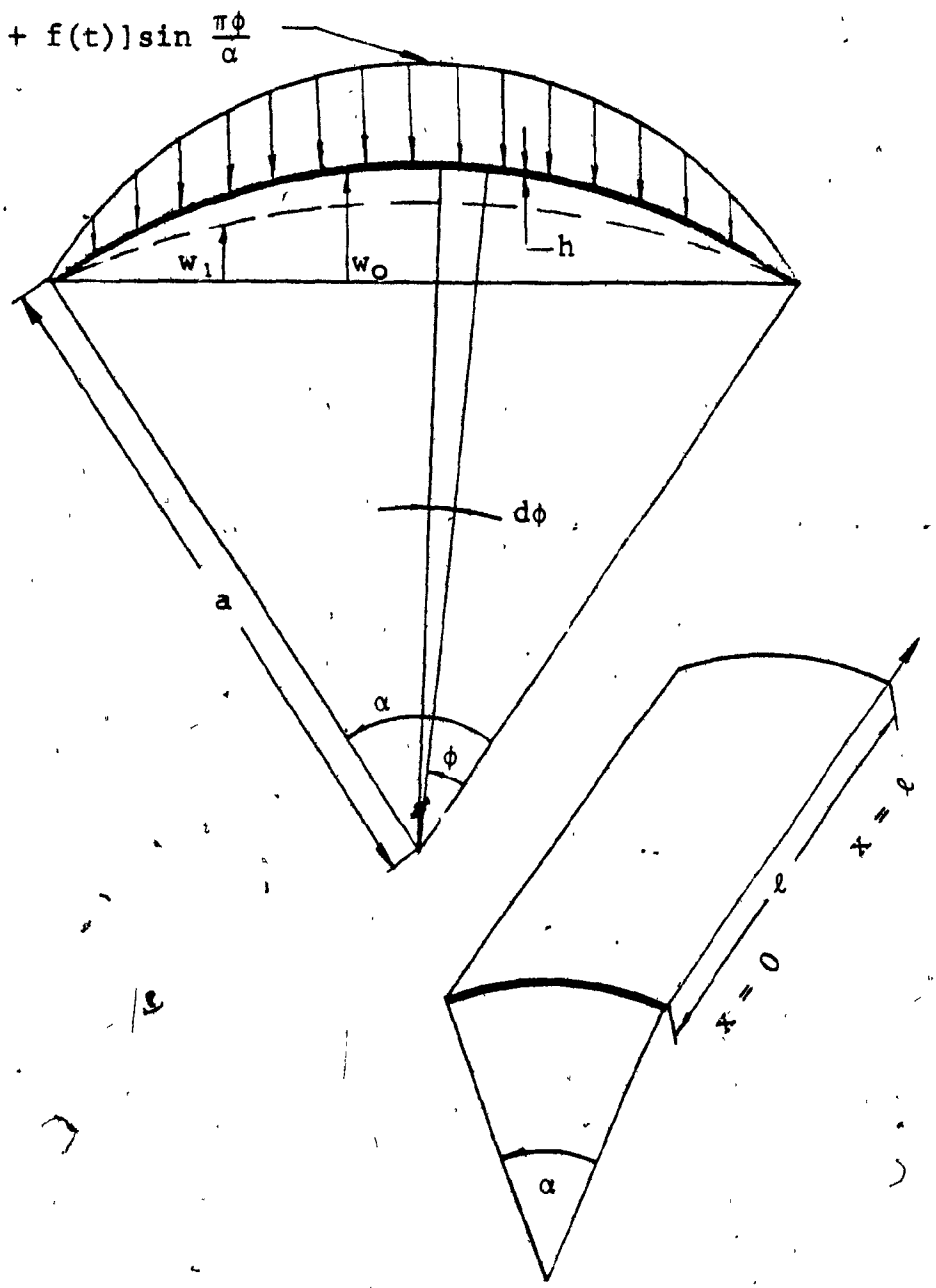

FIG. 4.1 Panel Geometry and Loading

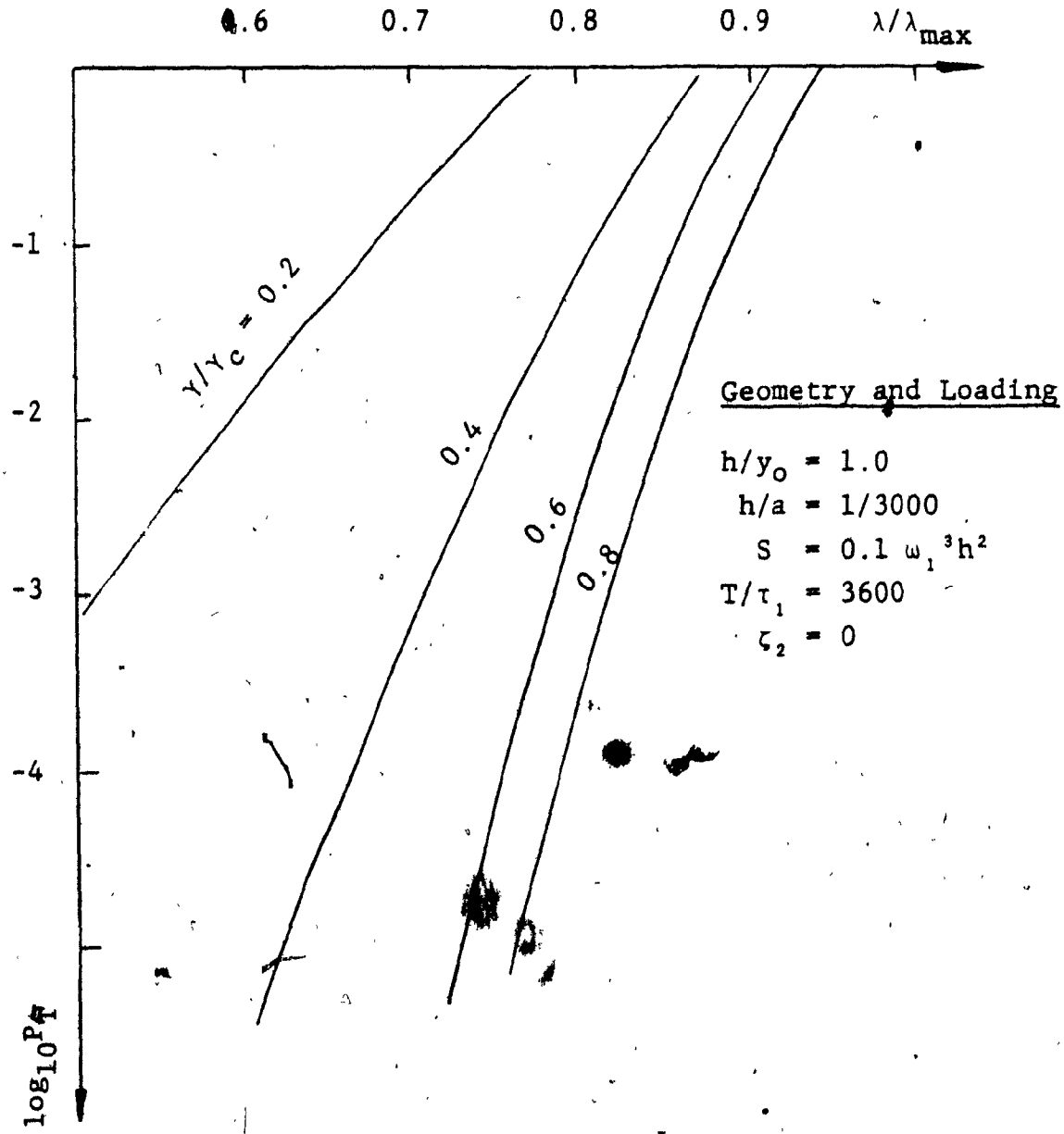

FIG. 4.2 Symmetric Buckling Probability

is enhanced by the introduction of small random disturbances, especially when λ approaches λ_{max}, due to the existence of the exponential term "$\exp(\frac{-2\ \gamma\ \omega_1\ H}{S})$" in equation (3.50). In laboratory and field testing where such structural systems are involved the previously described random disturbances do exist and may be attributed to the reported scatter of buckling loads [39]. These experimental critical loads are always found to be much lower than the theoretical critical loads.

Figure (4.3) gives results of asymmetric buckling probability for two-mode buckling of cylindrical panels. These results are similar to the symmetric snap-through results discussed earlier. In this case the panel is less shallow compared to the previous case so that the modes of deformation ζ_1 and ζ_2 are both real and distinct. The panel considered has $h/\bar{y}_o = 1/3$ and $h/a = 1/1000$ with all other conditions kept identical as before. In this case, the probability of failure by buckling shows similar characteristics to that shown in figure (4.2). In addition, it may be noted that the probability of buckling decreases with an increase in the shallowness of the panel.

For the same panel and using a reliability figure R_T in lieu of the probability of buckling P_T a set of plots can be drawn for design purposes. Figure (4.4) shows such a plot for a symmetric snap through problem. Assuming a load condition λ/λ_{max} of .75 it can be seen that for a damping of

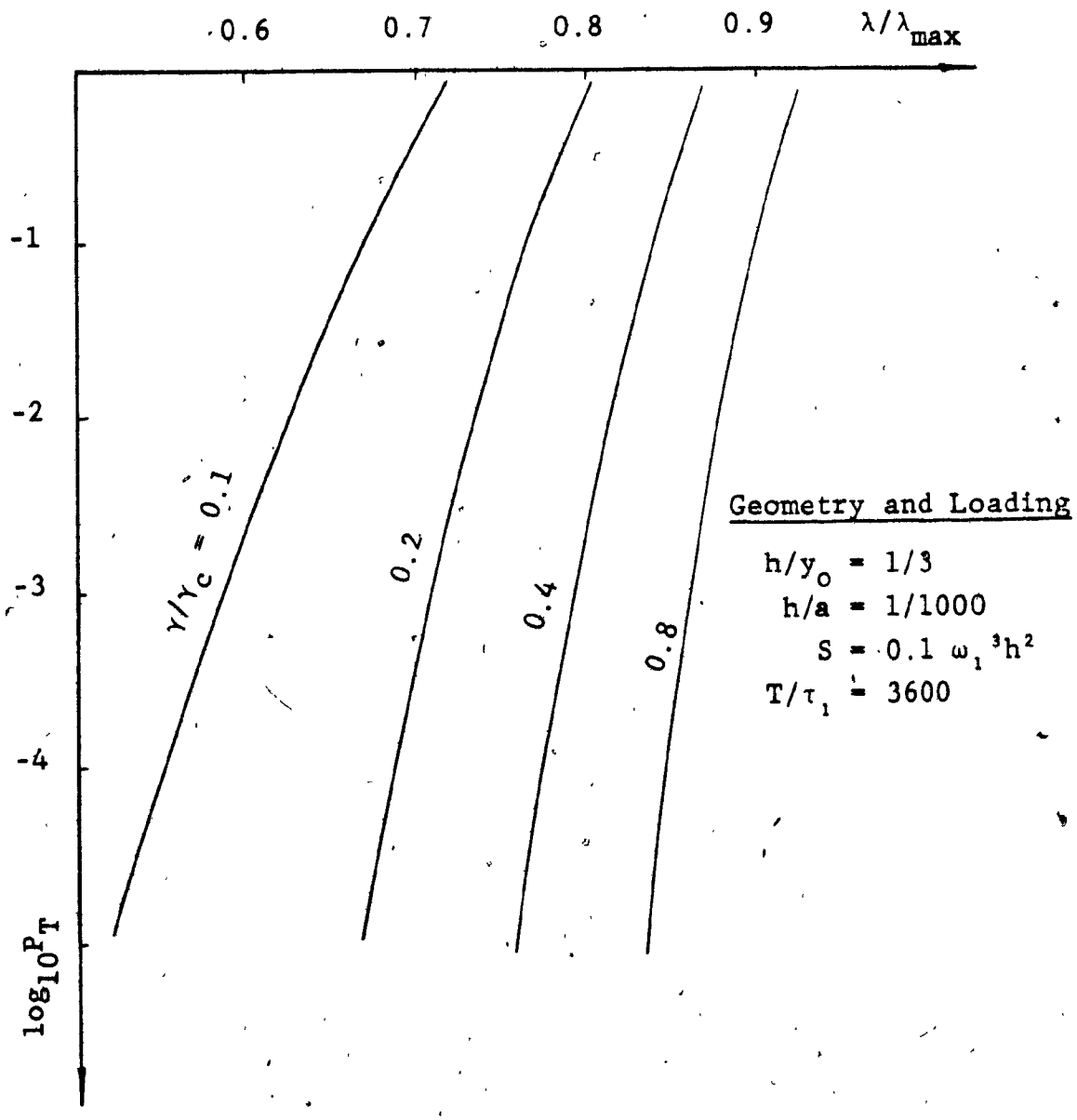

FIG. 4.3 Asymmetric Buckling Probability

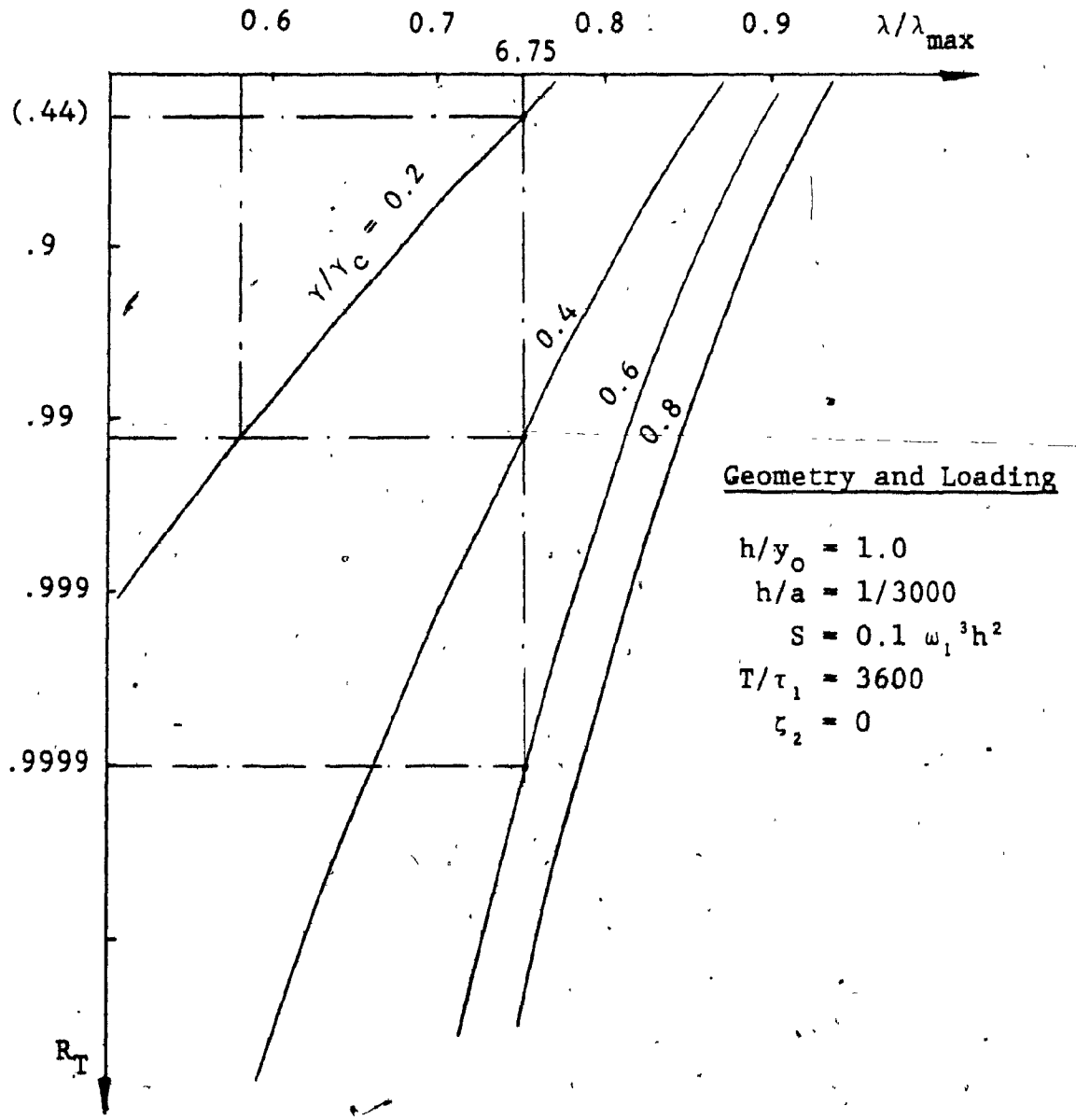

FIG. 4.4 Symmetric Buckling Reliability

$\gamma/\gamma_c = .2$ the reliability of the panel is $R_T = .44$ and a designer seeking a reliability figure of $R_T = .99$ can only achieve it by decreasing the load factor to $\lambda/\lambda_{max} = .59$ or by changing the damping ratio in his design to $\gamma/\gamma_c = .4$. On the other hand, if a reliability of $R_T = .9999$ is needed, only a design change involving a decrease in load combined with an increase in damping ratio can be considered other than a drastic change in the damping ratio, i.e. $\lambda/\lambda_{max} = .65$ with $\gamma/\gamma_{max} = .4$ or $\gamma/\gamma_c = .6$.

In the case of asymmetric buckling a similar set of plots is shown in figure (4.5). Again, for a load condition $\lambda/\lambda_{max} = .75$ a reliability factor $R_T = .99$ is reached with a damping ratio of $\gamma/\gamma_c = .21$ while a damping ratio of $\gamma/\gamma_c = .375$ is required to achieve with the same load a reliability of $R_T = .9999$. Showing clearly the effect of panel shallowness on the reliability factor.

4.5 Conclusion

Through this method, it is possible to generate a large family of plots such as in figures (4.2) through (4.5) giving the failure probabilities and the reliability of cylindrical panels for similar shell type structures under different mean load ratios. There curves can be effectively used as design charts for specifying the reliability of space enclosures for any given environmental loading pattern.

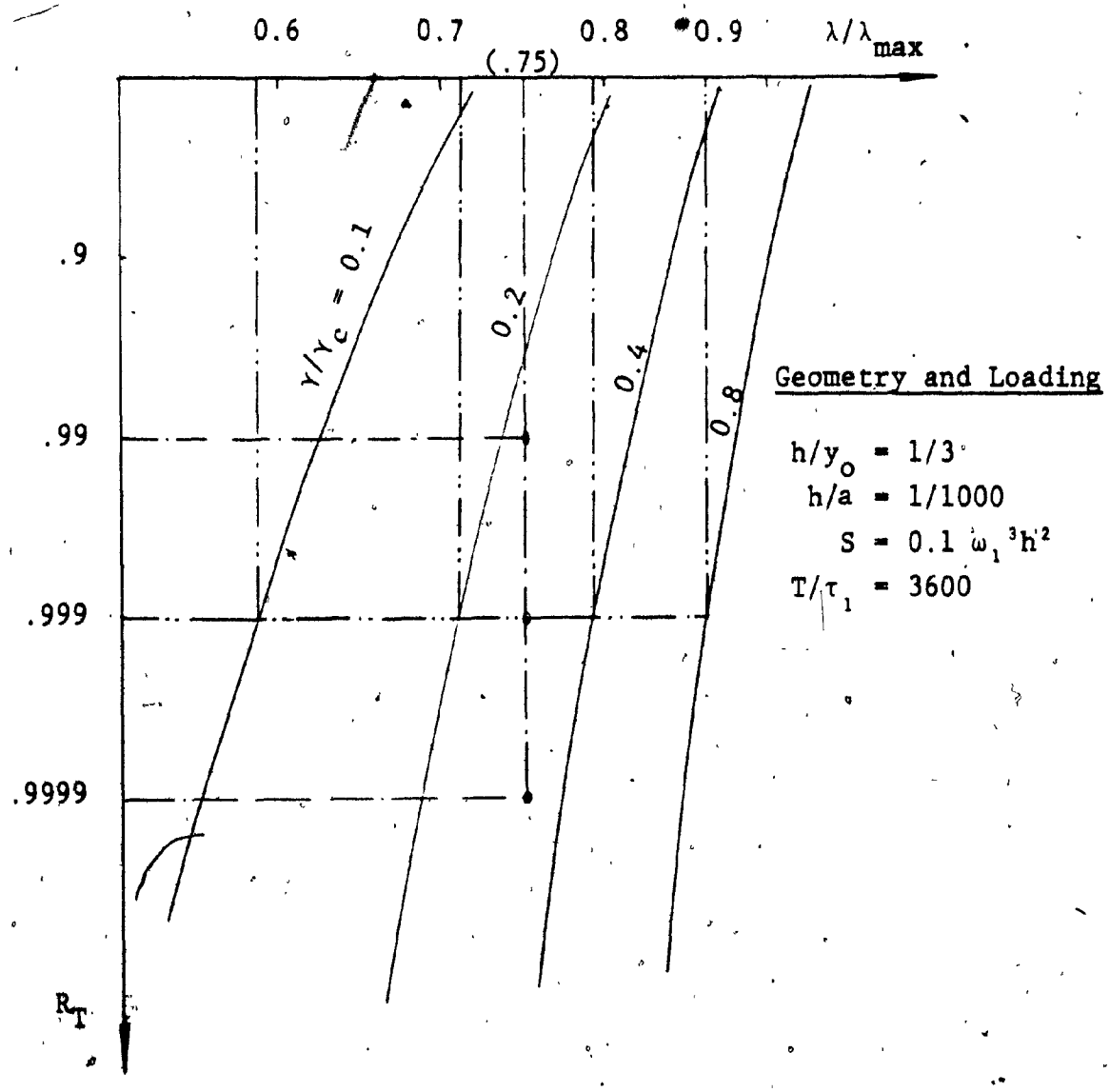

FIG. 4.5 Asymmetric Buckling Reliability

Actual designs in ships of all nature are based on maximum loading condition and panels are normally over-designed. With the Reliability approach using the first probability of buckling in a period of time the designs will become more effective and the structures will be lighter and more economical.

The difficulty of arriving at similar results in the case of spherical shells lies in the complexity of the energy equation (2.54) derived in Chapter II. Although difficult, it is possible to obtain a set of equations of motion by substituting equation (2.54) in the Lagrange's equations. Numerical solution of these equations for particular cases can be obtained using Newton-Raphson iteration process and Bushnell [32] computer program. The probability of first snap buckling as derived by Sankar and Ariaratnam [3] and shown in equation (3.22) can then be evaluated numerically. The length and complexity of this approach puts it beyond the scope of this report and is left as possible future investigation in this field.

CHAPTER V

CONCLUSION

Chapter V

CONCLUSION

In this report, the energy method is employed in order to extend the probabilistic analysis for evaluating the stability of three-dimensional space structures such as cylindrical panels and spherical shells under loading environments.

The problem of axisymmetric deformation of a shallow elastic spherical shell subjected to random external pressure, has been approached from the equilibrium and the potential energy point of views. The potential energy method is mainly used to determine the unstable portion of the load-displacement curve and it also allows for the introduction of imperfections in spherical caps.

The probability of failure by instability in a given time interval has been evaluated for a cylindrical panel of known properties and random load intensity. The application is then extended to include any general case of buckling where symmetric and asymmetric deformations are involved with different degrees of shallowness in the panel curvature.

Applications using numerical results computed for specific panels are discussed for the asymmetric and symmetric snap-through. The effect of the panel geometry on the determination of the mode of buckling is emphasized, illustrating the important role the shallowness of the structure

plays on the instability behaviour of the structure when subjected to stochastic load of given intensity.

The above analysis can be extended to other types of shell structures, namely spherical caps and shells using Newton-Raphson iteration process and Bushnell [32] computer program for solving the equilibrium equations.

The first probability of buckling under random loading constitutes in itself a new approach in the design of arches, panels, and shallow shells. Conventional design approach to a random loading, is mainly a fatigue failure analysis coupled with a maximum static buckling load resistance of the shell. This is in spite of the full awareness of the designers of the fact that the random loading is not necessarily subjecting the structure to a constant maximum load at all times.

By using the theory presented here for the first probability of buckling in a given time span, not only any brief peak load exposure is considered resulting in an increase in the life of the structure, but also resulting in an eventual decrease in the weight and manufacturing costs. At the same time the reliability of the structure can be approximately specified.

The first probability of buckling under random loading can become an effective design tool by generating large families of plots and graphs along the types illustrated in

this report. These sets of plots could reflect the reliability factors in terms of the first probability of buckling. Using non-dimensional factors the same curves could also be used for a variety of materials having a similar range of mechanical properties.

The approach itself can be extended to other types of shell structures. In such cases, the theory behind the analysis would be the same while the difference will be in the proper numerical analysis corresponding to each particular type of structure.

In order to bring out the merits of such reliability approach to design, it must be pointed out that it is not only enough to produce reliability design charts, but also to recognize as well, the types of loadings which can be considered as random, like pressure waves, gust loading due to winds, etc. In order to ensure the usefulness of the approach statistical data on such random loading experienced by structures have to be maintained, thus validating the results of similar designs. The analysis reported here for the probability of buckling uses stationary random loading but could eventually be extended to non-stationary random loading.

REFERENCES

1. Ariaratnam, S.T. and Sankar, T.S., "Dynamic snap-through of shallow arches under stochastic loads", AIAA Jnl., Vol. 6, No. 5, May 1968, pp. 798-802.

2. Sankar, T.S. and Ariaratnam, S.T., "Snap-buckling of shell-type structures under stochastic loading", Int. Jnl. of Solids Structures, Vol. 7, 1971, pp. 655-666.

3. Sankar, T.S. and Ariaratnam, S.T., "Instability of loaded shallow arches in non-symmetric modes", Int. Jnl. of Solids Structures, Vol. 7, 1971, pp. 1305-1316.

4. Lorenz, R., "Achsensymmetrische verzerrungen in dünn wandingen kohlzylindern", Zeitschrift des Vereines Deutcher Ingenieurs, Vol. 52, 1908, p. 1707.

5. Timoshenko, S., "Einige stabilitätsprobleme der elastizitätstheorie", Zeitschrift fur Mathematik und Physik, Vol. 38, 1910, p. 337.

6. Southwell, R.V., "On the general theory of elastic stability", Philosophical Transactions of the Royal Society of London, Series A, Vol. 213, 1914, p. 187.

7. Von Karman, T, and Tsien, H.-S., "The buckling of thin cylindrical shells under axial compression", Jnl. of the Aeronautical Sciences, Vol. 8, June 1941, p. 303.

8. Yoshimura, Y., "On the mechanism of buckling of a circular cylindrical shell under axial compression", Reports of Institute of Science and Technology of the University of Tokyo, Vol. 5, No. 5, Nov. 1951. (English translation available in "Technical Memorandum No. 1930 of the National Advisory Committee for Aeronautics", Washington, D.C., July 1955.)

9. Kirste, L., "Abwickelbare Verformung dünn wondiger Kreiszylinder", Desterreichisches Ingenieur-Archiv, Vol. 8, May 1954, p. 149.

10. Flügge, W., "Die Stabilität der Kreiszylinderschale", Ingenieur-Archiv, Vol. 3, 1932, p. 463.

11. Koiter, W.T., "Over de Stabiliteit van het elastisch Evenwicht", H.J. Paris, Amsterdam, Holland, 1945.

12. Koiter, W.T., "The effect of axisymmetric imperfections on the buckling of cylindrical shells under axial compression", Proceedings of the Royal Netherlands Academy of Sciences, Amsterdam, Series B, Vol. 66, No. 5, 1963.

13. von Karman, T. and Tsien, H.-S., "The buckling of spherical shells by external pressure", Jnl. of the Aeronautical Sciences, Vol. 7, Dec. 1939, p. 43.

14. Reissner, E., "On axisymmetric deformations of thin shells of revolution", Proceeding of Symposia in Applied Mathematics, American Mathematics Society, McGraw-Hill, Vol. 3, 1950, p. 27.

15. Krenzke, M.A. and Kiernan, T.J., "Elastic stability of near-perfect shallow spherical shells, AIAA Jnl., Vol. 1, 1963, pp. 2855-2867.

16. Donnell, L.H., "Shell theory", Illinois Inst. of Tech., DOMIIT Rep., No. 2-1, 1959.

17. Kaplan, A. and Fung, Y.-C., "A nonlinear theory of bending and buckling of thin elastic shallow spherical shells", NACA TN-3212, 1954.

18. Archer, R.R., "Stability limits for a clamped spherical shell segment under uniform pressure", Quarterly of Applied Mathematics, Vol. 15, No. 4, 1958, p. 355.

19. Simons, R.M., "A power series solution of the nonlinear equations for axi-symmetrical bending of spherical shells", Jnl. of Mathematics and Physics, Vol. 35, No. 2, 1956, p. 164.

20. Reiss, E.L., "On the nonlinear buckling of shallow spherical domes", Jnl. of the Aeronautical Sciences, Vol. 23, No. 10, 1956, p. 973.

21. Reiss, E.L., Greenberg, H.J. and Keller, H.B., "Nonlinear deflections of shallow spherical shells", Jnl. of the Aeronautical Sciences, Vol. 24, No. 7, 1957, p. 533.

22. Reiss, E.L., "Axially symmetric buckling of shallow spherical shells under external pressure", Jnl. of Applied Mechanics, Vol. 25, No. 4, 1958, p. 566.

23. Weinistschke, H.J., "On the stability problem for shallow spherical shells, Jnl. of Mathematics and Physics, Vol. 38, No. 4, 1960, p. 209.

24. Keller, H.B. and Reiss, E.L., "Spherical cap snapping", Jnl. of Aerospace Science, Vol. 26, No. 10, 1959, p. 643.

25. Keller, H.B. and Reiss, E.L., "Some recent results on the buckling mechanism of spherical caps", NASA TN-1510, 1962, p. 503.

26. Archer, R.R., "On the numerical solution of the nonlinear equation for shells of revolution", Jnl. of Mathematics and Physics, Vol. 41, 1962, p. 165.

27. Budiansky, B., "Buckling of clamped shallow spherical shells", Proc. Symp. Theory of Thin Elastic Shells, Delft, Aug. 1959, 1960, p. 69.

28. Murray, F.J. and Wright, F.W., "The buckling of thin spherical shells, Jnl. of Aerospace Science, Vol. 59, No. 5, 1961, p. 223.

29. Thurston, G.A., "A numerical solution of the nonlinear equations for axisymmetric bending of shallow spherical shells", Jnl. of Applied Mechanics, Vol. 28, 1961, p. 557.

30. Thurston, G.A., "Comparison of experimental buckling pressures for spherical caps", NASA TN-D 1510, 1962, p. 515.

31. Keller, H.B. and Wolfe, A.W., "On the non unique equilibrium states and buckling mechanism of spherical shells", Jnl. Soc. Ind. Appl. Mathematics, Vol. 13, No. 4, 1965, p. 674.

32. Bushnell, D., "Some problems in the theory of thin shells", Dissertation, Stanford University, Stanford, California, Feb. 1965.

33. Kramers, H.A., "Brownian motion in a field of force and the diffusion model of chemical reactions", Physica, Vol. 7, No. 4, 1940, pp. 284-304.

34. Goncharenko, V.M., "Study of the probability of snap-through of a long, cylindrical panel under random pressure", P.M.M., Vol. 26, No. 4, 1962, pp. 1107-1113.

35. Bushnell, D., "Nonlinear axisymmetric behavior of shells of revolution", AIAA Jnl., Vol. 5, No. 3, 1967, pp. 432-439.

36. Stratanovich, R.L., "Topics in the theory of random noise, Vol. 1, Gordon and Breach, 1963.

37. Madsen, W., Smith, L. and Hoff, N.J., "Automated derivation and integers representation of total potential and differential equation extension for assumed trigonometric series with an application to the post-buckling behavior of circular cylindrical shells", Stanford University, SUDAER report, No. 201, 1964.

38. Madsen, W., "Doctoral dissertation on post buckled characteristics of circular cylindrical shells", Stanford University, 1965.